HAL
open science

Self-Assembly in water of C60 fullerene into isotropic nanoparticles or nanoplatelets mediated by a cationic amphiphilic polymer

Théo Merland, Clément Drou, Stéphanie Legoupy, Lazhar Benyahia, Marc Schmutz, Taco Nicolai, Christophe Chassenieux

▶ To cite this version:

Théo Merland, Clément Drou, Stéphanie Legoupy, Lazhar Benyahia, Marc Schmutz, et al.. Self-Assembly in water of C60 fullerene into isotropic nanoparticles or nanoplatelets mediated by a cationic amphiphilic polymer. Journal of Colloid and Interface Science, 2022, 624, pp.537 - 545. 10.1016/j.jcis.2022.05.113 . hal-03805124

HAL Id: hal-03805124

https://hal.science/hal-03805124v1

Submitted on 25 Oct 2023

HAL is a multi-disciplinary open access archive for the deposit and dissemination of scientific research documents, whether they are published or not. The documents may come from teaching and research institutions in France or abroad, or from public or private research centers.

L'archive ouverte pluridisciplinaire **HAL**, est destinée au dépôt et à la diffusion de documents scientifiques de niveau recherche, publiés ou non, émanant des établissements d'enseignement et de recherche français ou étrangers, des laboratoires publics ou privés.

Table of contents

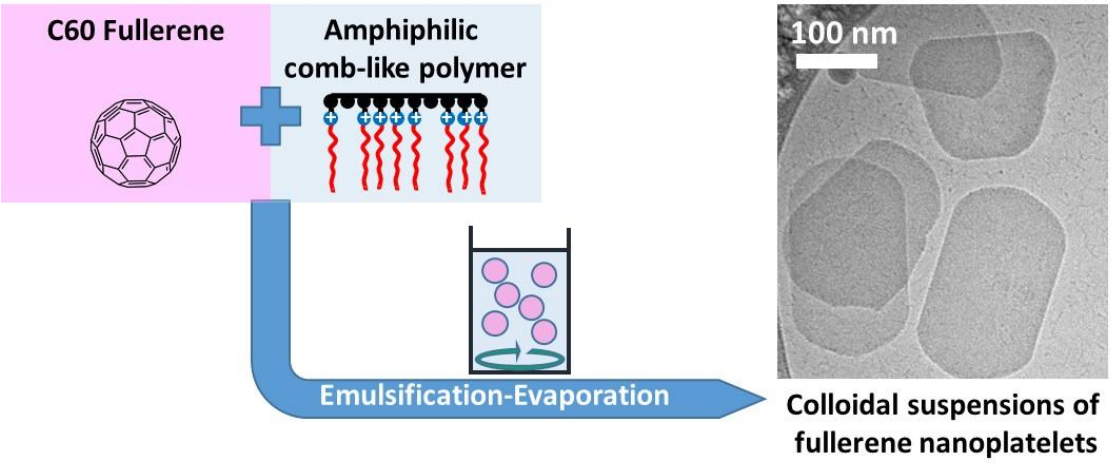

Self-Assembly in water of C_{60} fullerene into isotropic nanoparticles or nanoplatelets mediated by a cationic amphiphilic polymer

Théo Merland[a], Clément Drou[b], Stéphanie Legoupy[b], Lazhar Benyahia[a], Marc Schmutz[c], Taco Nicolai[a], Christophe Chassenieux[a]*

[a] Institut des Molécules et Matériaux du Mans, UMR CNRS 6283, Le Mans Université, Avenue Olivier Messiaen, 72085 Le Mans Cedex 9, France.

[b] Univ Angers, CNRS, MOLTECH-ANJOU, F-49000 Angers, France.

[c] Institut Charles Sadron, UPR CNRS 22, 23 Rue du Loess, 67034 Strasbourg Cedex, France.

E-mail addresses: theo.merland@univ-lemans.fr (T.Merland), clement.drou@univ-angers.fr (C. Drou), stephanie.legoupy@univ-angers.fr (S. Legoupy), lazhar.benyahia@univ-lemans.fr (L.Benyahia), marc.schmutz@ics-cnrs.unistra.fr (M. Schmutz), taco.nicolai@univ-lemans.fr (T. Nicolai), christophe.chassenieux@univ-lemans.fr (C. Chassenieux).

*Corresponding author: Christophe Chassenieux, IMMM - UMR CNRS 6283, Le Mans Université, Avenue Olivier Messiaen, 72085 Le Mans Cedex 9, France. Tel. (+33)2 43 83 39 12.

Abstract

Hypothesis: To disperse high concentration of C_{60} fullerene in water, we propose to use an emulsification-evaporation process in presence of an amphiphilic polymers whose chemical structure has been chosen for inducing specific interaction with fullerene The viscosity enhancement provided by self-assembly of the amphiphilic polymers in water should result in high stability of the suspensions. The organic solvent has also to been chosen so as to maximize the initial fullerene concentration.

Experiments: The concentrations of polymer and fullerene, the solvent type and the volume fraction of the organic phase have been varied. Their influence on the concentration of the fullerene dispersions and on the size and shape of the resulting nanoparticles have been investigated by UV-Visible spectroscopy, light scattering and cryo-transmission electron microscopy experiments.

Findings: The resulting nanoparticles consist of aggregates of C_{60} fullerene stabilized by the cationic polymer with morphologies/sizes tunable through fullerene and polymer concentration. At high fullerene concentration, nanoplatelets are obtained that consist in thin 2D nanocrystals. Their suspensions are very stable with time due to the viscosity of the dispersing aqueous medium. The concentration of fullerene nanoparticles dispersed in water is as high as 8g/L which corresponds to an upper limit that has never been reached so far.

Keywords: C_{60} fullerene, nanoplatelets, amphiphilic polymer, emulsification-evaporation, directed assembly

1. Introduction

The dispersion of C_{60} fullerene in water is a key issue due to numerous potential applications in medical[1-9] and materials sciences, [10-12] but remains a challenge because of the very hydrophobic nature of C_{60}.[13] It can be achieved through chemical modification of C_{60} with hydrophilic moieties.[14-20] As a result, the solubility in water can reach values as high as several hundreds of g/L as reported for fullerols.[21, 22] However, these chemical modifications involve tedious synthesis and purification steps[23] and affect the optical and biological activities of C_{60}.[18, 22] To overcome these difficulties, dispersion of neat C_{60} fullerene in water has been attempted using various processes. Many of them imply the solubilization of C_{60} in an organic solvent followed by transfer to water and removal of the organic solvent leading to aqueous colloidal suspensions of fullerene. The solvent transfer can be achieved in different ways: i) emulsification in water of a solution of fullerene in an

organic solvent not miscible with water,[5, 24] ii) successive transfers of solvents from organic apolar solvents to organic polar ones and then to water by successive matching of miscibility,[24, 25] iii) nanoprecipitation/dialysis into water using a water-miscible organic solvent.[26, 27] These methods yielded particles with various morphologies. Nanoprecipitation from THF produced faceted 3D nanocrystals,[28] while sonication of toluene/water emulsion led to amorphous spherical particles.[6] Beside the morphology of the colloids that can be produced, a key parameter that has deserved much attention is the maximum concentration of fullerene that can be dispersed in water and which often requires the assistance of a polymer. Up to 0.6 g/L of fullerene can be dispersed in water by nanoprecipitation through the use of pullulan bearing cholesteryl groups, which acts as a stabilizer [29] and up to 1.3 g/L in the presence of a peptide.[30] The efficiency of the emulsification-evaporation method to disperse fullerene has not been studied much, but it was found at best to be 1.4 g/L.[31, 32] Furthermore, the emulsification-evaporation method has already proven to be up-scalable and was used to produce inks for photovoltaic devices. [33, 34]

Generally, the use of molecular or polymeric surfactant is required to obtain concentrations of fullerene dispersed in water higher than a few ppm.[35-37] In the present study, we used an amphiphilic polymer (noted 75C12) consisting of a polystyrene backbone bearing surfactant-like moieties (**Figure 1**). It has already been shown that this polymer is able to efficiently disperse nanoparticles such as quantum dots, both in aqueous solution and in bulk material [38-40] and to stabilize as well latex particles obtained by emulsion and mini-emulsion radical polymerization.[41] Based on its chemical structure, both hydrophobic and π-stacking interactions are expected to occur with C_{60}. In aqueous solution, it has been reported that neat 75C12 self-assembles into worm-like micelles that branch and form a percolating network at higher concentrations. [42]

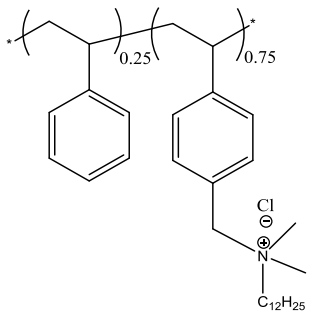

Figure 1. Chemical structure of the amphiphilic copolymer 75C12, 75 stands for the relative molar ratio in % of cationic moieties which contain dodecyl (C12) side chains.

In this paper, we report on the formation of C_{60} nanoparticles in water assisted by 75C12 *via* an emulsification-evaporation process. The amount of fullerene transferred into water was quantified using UV-spectroscopy. The dispersed nanoparticles were characterized in terms of size, molar mass, morphology, and stability. We will show that the processing parameters (type of solvent, fullerene and polymer concentrations, phase volume fractions) strongly influence the concentration and the type of fullerene nanoparticles that are dispersed in water. The maximum concentration of fullerene nanoparticles that could be dispersed in water in this manner was 8 g/L, which is six times higher than the highest value reported so far. We will show that in some cases fullerene nanocrystals are formed in the form of elongated thin platelets.

2. Experimental Section/Methods

Materials: Toluene (Fischer Scientific, analytical reagent grade), chloroform (Sigma-Aldrich, >99.0%), carbon disulfide (Sigma-Aldrich, >99.9) and ultrapure water (Millipore) were used as received. C_{60} fullerene (purity 99.9%) was purchased from MST-Nano Co., Ltd. (Saint-Petersburg, Russia) and dissolved either in chloroform, toluene or carbon disulfide by magnetic stirring during 24 hours in brown vials in order to protect them from light. These solutions were stored in the dark at room temperature prior the emulsification steps. Saturation concentrations were determined by UV-visible spectroscopy.

Polymer synthesis: The synthesis has been already described. [43]In this work, a copolymer with 75%mol cationic units with C12 pendant alkyl chains was obtained, with $M_n = 4.10^4$ g/mol and Đ=1.5 as determined by size exclusion chromatography and light scattering experiments. Same micro- and macroscopic behavior were found as for the polymer 80C12 described elsewhere.[42, 43] The polymer solutions were prepared in water or in chloroform by dissolving it at 80°C or 20°C respectively during 15 hours.

Preparation of the C_{60} dispersions in water: 4 mL of mixtures of aqueous and organic phases and with various composition (see table 1) were sonicated with an ultrasound horn tip at frequency of 20 kHz at 36% amplitude in continuous mode. It resulted in emulsions that were further sonicated until the organic solvent was fully removed by evaporation after a few minutes.

Extraction of C_{60} from water: In order to quantify the amount of fullerene that was dispersed in water (see main text), it was extracted from water into toluene according to Deguchi et al. [27]1 mL of aqueous suspension was mixed with 1 mL of 1%wt of NaCl and 2 mL of toluene. After stirring, the aqueous phase turned from yellow to colorless, and the extraction from water to toluene was proven to be complete by checking the absence of any trace of fullerene

in water by UV-vis. The extinction coefficient for fullerene in toluene was determined experimentally using Beer-Lambert law for solutions of known concentration. and was found to be equal to 87 L/g/cm at 336 nm (see Figure S7b).

UV-visible spectroscopy: The absorbance was measured as a function of the wavelength between 200 nm and 800 nm in quartz cuvettes with an optical path length of 1 cm using a Cary 50 Bio spectrophotometer (Varian Medical Systems, Palo Alto, CA, USA).

Differential refractometry: The refractive index increments (dn/dC) were measured with an Optilab refractometer (Wyatt Technology, Santa Barbara, CA, USA) using an emulsion without any polymer and fullerene treated in the same manner as a blank. Dispersions with various concentrations were analysed. The refractive index increment (dn/dC) of fullerene in water was determined using a sample without polymer. It was found to be equal to 1 mL/g (Figure S9a), which is much higher than dn/dC = 0.19 mL/g reported for 75C12 in water. [42]For a dispersion containing both polymer and fullerene derived from M5, the measured dn/dC was equal to the weighted average of that of C_{60} and 75C12 (Figure S9b).

Light scattering: Measurements were done at *T*=20°C on a CGS-3 (ALV GmbH, Germany) compact system with an LSE-5004 correlator. The scattering angle (θ) was varied from 12° to 150° and the wavelength of the laser (λ) was 632.8 nm. The scattering wave vector q is given by q=4π.n.sin(θ/2)/λ, with n the refractive index of the solvent. Static Light Scattering (SLS) was performed to measure the Rayleigh ratio (R_θ) of the dispersions according to:

$$R_\theta = \frac{I_{solution} - I_{solvent}}{I_{ref}} \times R_\theta^{ref} \quad (1)$$

where $I_{solution}$, $I_{solvent}$ and I_{ref} stand for the scattering intensity of, respectively, the dispersion, the solvent and toluene which is used as a reference with $R_\theta^{ref}=1.35.10^{-5}$ cm^{-1}.

At low concentrations where the effect of interactions can be neglected R_θ is related to the weight average molar mass (M_w) and the z-average radius of gyration (R_g) of the solute:

$$\frac{KC}{R_\theta} = \frac{1}{M_w}\left(1 + \frac{q^2 {R_g}^2}{3}\right) \quad (2)$$

K is an optical constant defined as:

$$K = \frac{4\pi^2 {n_{ref}}^2 \left(\frac{dn}{dC}\right)^2}{N_A \lambda^4} \quad (3)$$

with n_{ref} the refractive index of toluene and N_A Avogadro's constant.

With Dynamic Light Scattering (DLS) one measures the autocorrelation function $g_1(t)$ that was fitted to a distribution of relaxation times (τ) using the REPES routine:[44]

$$g_1(t) = \int A(\tau) \exp\left(-\frac{t}{\tau}\right) d\tau = \int A(\tau) \exp(-D.q^2.t)\, d\tau \quad (4)$$

In dilute solutions where the effect of interactions can be neglected and for particles smaller than q^{-1}, the relaxation is due to their translational diffusion and τ is related to the diffusion coefficient (D) as: $\tau = 1/(Dq^2)$. The hydrodynamic radius (R_h) can be calculated from D using the Stokes-Einstein equation:

$$D = \frac{kT}{6\pi\eta_s R_h} \quad (5)$$

with k the Boltzmann constant, T the temperature and η_s the viscosity of the solvent. Typical distributions of sizes are shown in **Figure S19** for dispersions prepared with methods M1, M2 and M3. At low C_{pol}, a single population is observed, with a size distribution that broadens with increasing C_{pol} and shifts toward lower R_h values. For C_{pol} ≥10 g/L, two populations could be distinguished, but we have only considered the size of the fast mode of relaxation, the slow one corresponding to scatterers with concentration that can be neglected. In this specific case, the polymer contribution could no longer be neglected and the weight-averaged dn/dC of both 75C12 and C_{60} was used. For samples prepared with method M4 and M5, a single population was observed whatever C_{pol}. So as to neglect the interactions, prior their light scattering investigation samples were diluted down to 5 mg/L fullerene with NaCl solution (5 mM).

Cryo-TEM: A lacey carbon film (Ted Pella) is rendered hydrophilic with a glow discharge (Elmo-Cordouan Technologie) just before depositing 5µL of the solution. The solution is blotted to form a thin film with a home-made freezing machine (*T*=22°C and humidity 80 % RH) and the grid is plunged rapidly in a liquid ethane bath maintained at liquid nitrogen ebullition point. The water film is forming an amorphous ice layer in which the structures are well preserved in their native state. The grid is transferred under liquid nitrogen on a Gatan 626 cryo holder and transferred into the TEM (Tecnai G2 sphera FEI). The grids are observed under low dose conditions at 200 kV and images taken with an Eagle 2K ssCCD camera (FEI).

Confocal microscopy: Confocal Laser Scanning Microscopy pictures were taken with a Zeiss LSM 800 (Carl Zeiss Microscopy GmbH, Germany). One drop of a 1 g/L solution of Rhodamine B was added to the samples prior dispersion. After the latter step, one drop of emulsion was placed on a glass slide and sealed with a cover slip. We hypothesize that the chromophore preferentially labels the polymer because of the presence of rings around the droplets. Pictures of 512x512 pixels were taken with a water-immersion objective HC × PL APO 63 × NA=1.2 and a magnification of 1. The incident laser beam had a wavelength of 548 nm and the fluorescent light was collected between 560 and 700 nm.

3. Results

3.1. Preparation of aqueous C_{60} colloidal suspensions

Dispersions of C_{60} in water were prepared by modifying the emulsification-evaporation method reported for toluene/water by Andrievsky et al. [45] and using also chloroform ($CHCl_3$) and carbon disulfide (CS_2) for solubilizing C_{60}. C_{60} has widely different solubility values in these solvents (the limit solubility for C_{60} being 90 mg/L, 2.8 g/L and 7.6 g/L respectively for $CHCl_3$, toluene and CS_2) and display lower boiling points than toluene. The C_{60} concentration in $CHCl_3$ was set at 0.09 g/L, whereas three concentrations were tested in CS_2 (0.09, 1 and 7.6 g/L). 75C12 is soluble in $CHCl_3$, but not in CS_2 nor in toluene. For the former solvent, we then tested the effect of adding 75C12 dissolved initially in the aqueous phase or in the organic phase. For the other solvents, the cationic amphiphilic polymer 75C12 was added to the aqueous phase at concentrations between 35.10^{-3} and 35 g/L. The different conditions tested here are summarized in **Table 1**. The volume fraction of the organic phase (Φ_{org}) was 25% when not specified, but for two methods, it was varied between 10 and 75%.

Table 1. Summary of the various conditions used to disperse C_{60} in water.

Method	Organic solvent	Polymer concentration[a)] (g/L) / solvent	C_{60} concentration in organic phase (g/L)	Volume fraction of organic phase
M1	$CHCl_3$	1.10^{-3} to 35 / $CHCl_3$	0.09[b]	25%
M2	$CHCl_3$	35.10^{-3} to 35 / H_2O	0.09[b]	25%
M3	CS_2	35.10^{-3} to 35 / H_2O	0.09	25%
M4	CS_2	0.35 to 35 / H_2O	1	25%
M5	CS_2	1 to 35 / H_2O	7.6[b]	25%
M6	CS_2	35 / H_2O	7.6[b]	10 to 75%
M7	CS_2	10 / H_2O	7.6[b]	10 to 75%

[a)] Final concentration in water after evaporation of the organic solvent; [b)] saturation concentration for C_{60} fullerene in the organic phase.

The organic and aqueous phases were mixed and emulsified with an ultrasound horn tip, as described in the experimental section. In all cases, the emulsions consisted of droplets of the organic phase embedding C_{60} dispersed in a continuous aqueous phase. The morphology of the emulsions was inspected using confocal laser scanning microscopy (CLSM) as described in the experimental section. Examples for different systems are shown in the supplementary information (**Figures S1 to S5**). In all cases, droplets with diameters between 1 µm and 10

µm were formed. Sonication led to an increase of the temperature to about 80°C within 5 minutes and consequently to evaporation of the organic solvent. It was found that with increasing sonication time the droplet size decreased until complete evaporation of the organic solvent, which could take up to 6 min for CS_2 and 10 min for $CHCl_3$. We noted that at high 75C12 concentrations (10, 35 g/L) all of the organic phase was emulsified within 1 min of sonication. However, at lower concentrations (1 g/L) complete emulsification took longer and occurred while the solvent was evaporating. The color of the final aqueous dispersions ranged from faintly yellow to dark brown, depending on the concentration of dispersed fullerene, see **Figure S6**.

3.2. UV-visible light absorption of C_{60} dispersed in water

Figure S7a displays a typical UV-visible absorption spectrum for an aqueous dispersion of C_{60}. In the UV region, two bands were observed at 260 nm (I) and 340 nm (II) as well as a broad band with low amplitude close to 440 nm (III). An absorption band was also observed at 220 nm but since the polymer absorbs strongly at this wavelength, we will not consider it in the following. For the other wavelengths, the absorbance spectra have been corrected for the contribution of the polymer in order to recover the sole fullerene absorption spectrum, see Figure S7a. The absorption spectrum of C_{60} dissolved in toluene is shown in **Figure S7b** and shows a single absorption band at 336 nm.

The absorption peak II is used in the literature to quantify the concentration of C_{60} dispersed in water. However, the reported values of the extinction coefficient vary a lot between different authors (Andrievsky=94.4,[31] Deguchi=71.2,[27] Scharff=5.62,[46] Chen=26.3 [47] L/g/cm). Here, we determined the C_{60} concentration for a range of aqueous C_{60} dispersions by extraction into toluene[27] and measuring the absorbance at 336 nm using the experimentally determined extinction coefficient ε=87 L/g/cm. Knowing the C_{60} concentration, we have determined an average value for the extinction coefficient at 340 nm ε = 105±15 L/g/cm, which is close to the value reported by Andrievsky et al.[31]. In the following, we used this extinction coefficient for determining the amount of the fullerene dispersed in water which was further confirmed by extraction into toluene.

3.3. Concentration of C_{60} in water

Figure 2a displays the concentration of C_{60} (C_{full}) that could be dispersed in water as a function of the concentration of 75C12 (C_{pol}). C_{pol} was kept lower than 35 g/L, because at higher concentrations 75C12 forms a gel in aqueous solution. In **Figure S8c**, the same data

are plotted in terms of the yield defined as the ratio between C_{full} and the theoretical C_{60} concentration if all C_{60} in the emulsion had been effectively dispersed. The reproducibility of the results can be judged from the spread of the data shown in Figure 2 when obtained at the same conditions. The amount of C_{60} that dispersed in water increased with increasing 75C12 content until it reached a plateau value. For a given C_{60} concentration in the organic phase (90 mg/L), the same plateau value was reached but at a lower polymer concentration for chloroform than for CS_2 (see **Figures S8a and S8b**) and much less polymer was needed to reach the plateau if it was dissolved in chloroform together with the C_{60}. If more C_{60} was dispersed in CS_2, then more polymer was needed in the aqueous phase to reach the plateau. The maximum amount of C_{60} that could be dispersed depended on the C_{60} concentration in the organic phase, but not on the type of solvent. However, the maximum yield was found to be between 70 and 90% independent of the C_{60} concentration whether in $CHCl_3$ or in CS_2, see **Figure S8b-c**. At best, a fullerene concentration equal to 2.3 g/L was obtained with method M5 and C_{pol}=35 g/L.

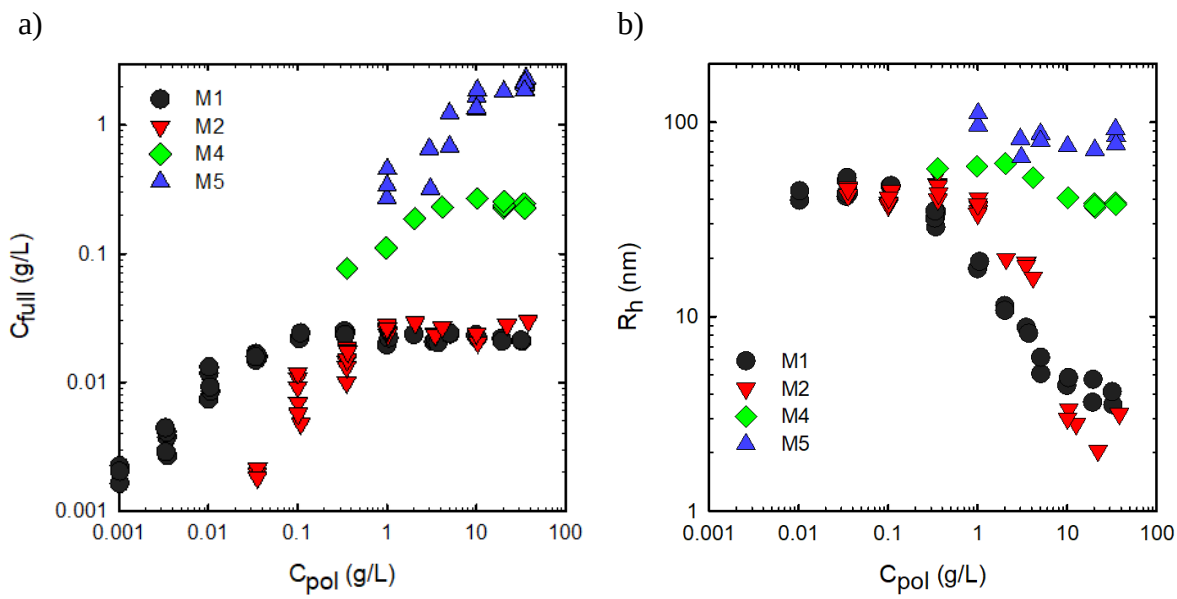

Figure 2. Concentration (a) and hydrodynamic radius (b) of fullerene nanoparticles dispersed in water as a function of the polymer concentration and with different methods of dispersion as indicated in the legend of the figure.

3.4. Size and molar mass of the C_{60} particles

The average molar mass (M_w), radius of gyration (R_g) and hydrodynamic radius (R_h) of the dispersed C_{60} particles were determined by static and dynamic light scattering techniques, as described in the experimental section. The contribution of the polymer to the scattered light compared to that of the C_{60} particles was in most cases negligible, because the contrast of the

latter was 25 times larger (see **Figure S9**). R_g was found to be proportional to R_h with $R_g/R_h \approx 1.3$, see **Figure S10a**. Here we will discuss only R_h that can be determined accurately over a wider range of particle sizes, but the influence of C_{pol} on both R_g and M_w is also reported in the supporting information (see **Figure S11**). For dispersions prepared from chloroform, R_h was comprised between 40 and 50 nm at low polymer concentrations whatever the initial location of the polymer (M1, M2), see **Figure 2b**.

This size is much larger than an individual fullerene molecule, which has a radius of 0.35 nm, indicating that aggregates were formed. Upon further increasing C_{pol}, R_h decreased by almost one order of magnitude, down to a few nanometers. It should be noted that the R_h of 75C12 in dilute aqueous solution is approximately 4 nm,[42] i.e. similar to R_h observed here at higher polymer concentrations. It is possible that at these high polymer concentrations and small particle size, the contribution of the polymers can no longer be neglected. The size of the particles in dispersions prepared from CS_2 at the same fullerene concentration as in chloroform (M3, see **Figure S10b**) also displayed a significant decrease with increasing C_{pol}, but the decrease started at higher C_{pol}. When the fullerene concentration in CS_2 was increased to 1 g/L (M4), the size of the particles decreased only weakly with increasing C_{pol} from about 60 nm to about 40 nm. With 7.6 g/L (M5) R_h varied between 60 nm and 100 nm, but did not depend systematically on C_{pol}.

3.5. Influence of the volume fraction of the organic phase

The effect of the volume fraction of the organic phase (Φ_{org}) was studied using saturated solutions of C_{60} in carbon disulfide and aqueous solutions of 75C12 at fixed concentrations of 35 (M6) and 10 g/L (M7). **Figure 3a** shows that the amount of fullerene that was dispersed in the aqueous phase increased strongly with increasing Φ_{org} up to about 40% and then either reached a plateau around 4 g/L for M7 or increased weakly up to 8 g/L at Φ_{org}=75% for M6. Please note that this values are far above ones that has been reported so far in the literature as stated in the introduction. The yield increased with increasing Φ_{org} until it reached a maximum between Φ_{org}=25% and 40% at C_{pol}=35 g/L and closer to Φ_{org}=40% at C_{pol}=10 g/L (see **Figure S12a**). In spite of the decreasing yield, the actual concentration of fullerene in the aqueous dispersion did not decrease at higher Φ_{org}, because the decrease of the yield was compensated by the decrease of the volume fraction of the water phase.

The influence of Φ_{org} on the hydrodynamic radius of the particles is plotted in **Figure 3b**. For both polymer concentrations, the smallest sizes were observed when $\Phi_{org} \leq 25\%$. At higher Φ_{org} the size increased by approximately a factor 2. Particles prepared at C_{pol}=35 g/L were

systematically larger than the ones prepared at C_{pol}=10 g/L. Φ_{org} influences both R_g and M_w in the same way as for R_h (**Figure S13**).

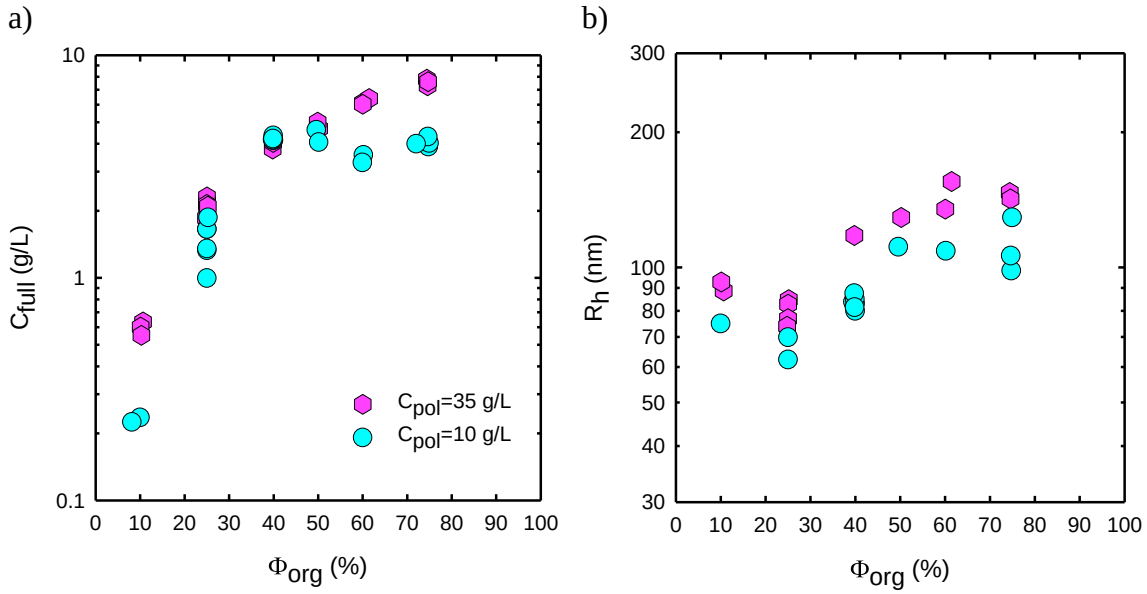

Figure 3. Concentration of fullerene particles dispersed in water (a) and their hydrodynamic radius (b) as function of the volume fraction of CS_2 for methods M6 and M7. The polymer concentration in the aqueous phase is indicated in the figure.

3.6. Stability of the fullerene dispersions

The extent of sedimentation of C_{60} under gravity with time was studied by measuring the concentration of C_{60} in the supernatant for samples prepared from method M5 with C_{pol} varying from 1 g/L to 35 g/L, results are reported in **Figure S14.** During more than 2 months, samples at C_{pol}=1 and 35 g/L remained very stable showing almost no sedimentation under gravity. However, at C_{pol}=10 g/L, C_{full} decreased by a factor of 2 during the same ageing time most likely due to slow aggregation of the particles. The latter being slowed down at C_{pol}=35 g/L, due to the self-assembly of 75C12 resulting in viscosity of the continuous phase two orders of magnitude higher than at 10 g/L[48] The destabilisatioon of samples with C_{pol}=10g/L can be however prevented by decreasing the concentration of fullerene particles in the dispersion that is by diluting it with 75C12 at the same concentration than in the continuous phase see **Figure S14b.** We note that simple handshaking of the samples led to complete redispersion of the particles that had sedimented which hints at its reversible temper.

3.7. Morphology of the C_{60} particles

Figure 4 shows the relationship between M_w and R_h for fullerene nanoparticles prepared with various methods. Within the scatter, a power law $M_w \propto R_h^3$ was found for R_h>30 nm, which

would mean that these particles had approximately the same density whatever their size. The smaller particles deviated upward from this behavior indicating that they were denser.

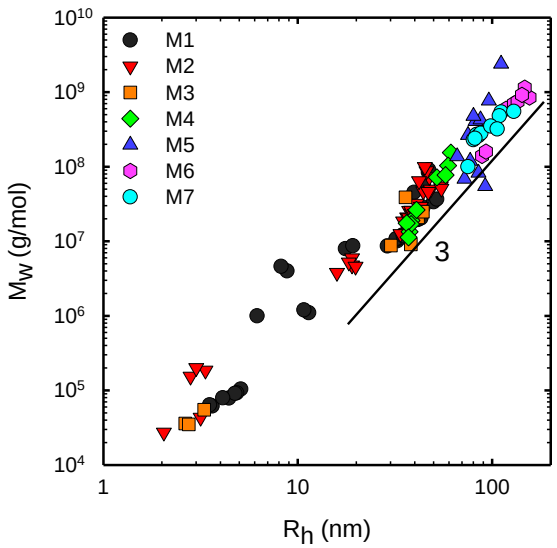

Figure 4. Weight average molar mass of fullerene particles as a function of their hydrodynamic radius.

The dispersity of the particles size has been evaluated by sequentially filtrating the samples on membranes with various porosity. After each filtration step, UV-visible absorption spectra were collected in order to determine the fullerene concentration, see **Figure S15**. It appeared that the dispersity increased when C_{pol} was increased, see **Figure S16**.

Cryo-TEM images of C_{60} particles dispersed in water using method M5 with C_{pol}=10 g/L are shown in **Figures 5a** and **S17**. We can distinguish two kinds of structures. The first one indicated by the long black arrow in Figure 5a are thin faceted platelets displaying some crystalline order. A few particles display some twinning as can be seen in **Figure 5b**. The second kind of structures (short black arrow) are thicker objects. In a few of them, small white spots can be seen that may have been caused by beam damage though the images were taken under low dose conditions. Alternatively, they can represent small defects in the crystal. In both cases, it could indicate the presence of 75C12 macromolecules inside the structures. In the amorphous water layer, worm-like micelles (WLM) are observed at higher defocus values (short white arrow) corresponding to self-assembled 75C12 in water. [42] The long white arrow corresponds to the Carbon-Formvar lacey supporting film. Similar morphologies for the fullerene nanoparticles are observed for dispersions formed with method M7 with C_{pol}=35 g/L and Φ_{org}=75% (Figure 5b). WLM are less visible in Figure 5b because the images were taken at a lower defocus value. When Φ_{org} was decreased from 25% to 10%, only a small number of

isotropic objects are seen (short black arrow in **Figure 5c**). The majority of objects are the WLM (white short arrow in Figure 5c). Dispersions prepared with method M4, i.e. starting with less fullerene, with C_{pol}=10 g/L also displayed only a few small platelets together with small isotropic particles (**Figure 5d**). Dispersion made with method M1 with C_{pol}=10 g/L only contained small isotropic particles (**Figure S18a**) as did a dispersion that contained no polymer (**Figure S18b**).

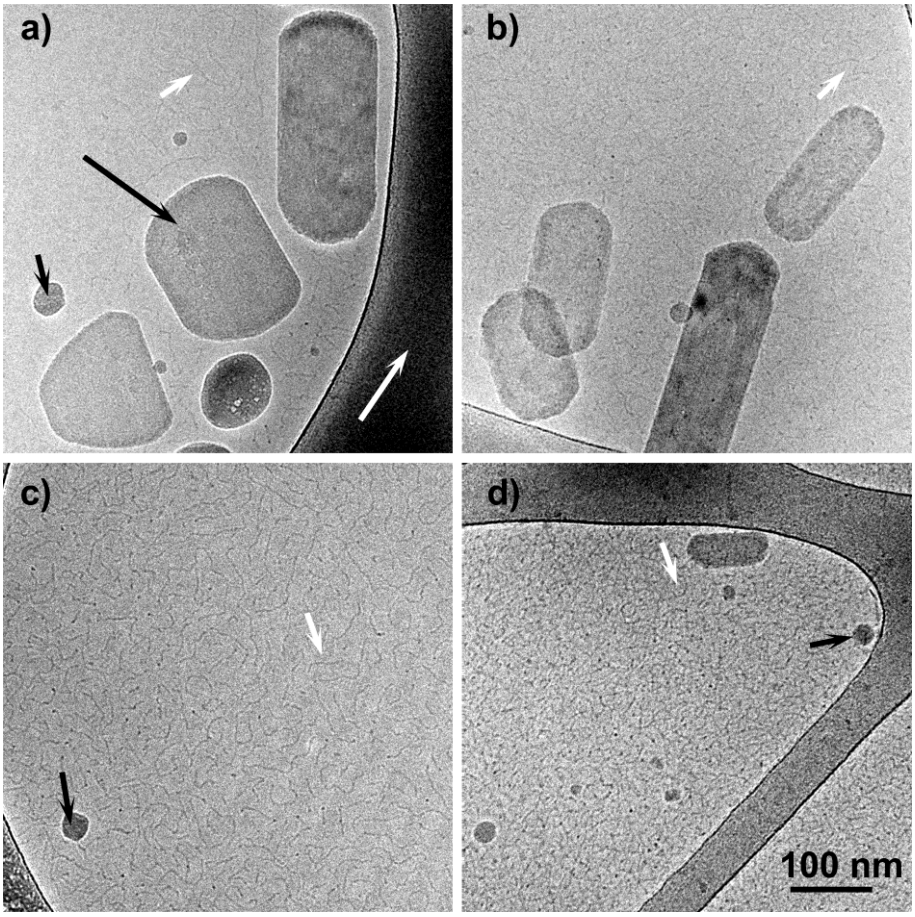

Figure 5. Cryo-TEM pictures for samples a) M5 (C_{pol}=10 g/L, Φ_{org}=25%), b) M7 (C_{pol}=35 g/L, Φ_{org}=75%), c) M6 (C_{pol}=35 g/L, Φ_{org}=10%) and d) M4 (C_{pol}=10 g/L, Φ_{org}=25%). Short white arrows indicate polymeric worm-like micelles; the long white arrow shows Carbon-Formvar lacey supporting film; short black arrows show small isotropic fullerene particles; the long black arrow shows a fullerene nanoplatelet.

4. Discussion

The emulsification/evaporation process in combination with an amphiphilic cationic polymer (75C12) has allowed by tuning both the nature and volumic fraction of the organic phase and the concentration of polymer to disperse as high as 8g/L of C_{60} fullerene in the form of nanoparticles either isotropic or in the form of nanoplatelets. To account for such a result, we

propose the following mechanism (see **Scheme 1)**. Fullerene is initially dissolved molecularly in the solvent which is latter on dispersed in the form of droplets in the aqueous phase by ultrasonication. Ultrasounds also heat the emulsions causing evaporation of the solvent. When the latter evaporates, the concentration of fullerene exceeds its limit of solubility leading to nucleation and growth of C_{60} particles. As the droplets are orders of magnitude larger than these particles (see Figures S1 to S5), it is clear that many nuclei are formed in each droplet and then further grow and diffuse under Brownian motion within the droplets. When the particles come in contact with the polymer, the latter binds to them. With chloroform, this can occur inside the droplet or at the solvent/water interface, since the polymer is soluble in both $CHCl_3$ and water. However, when CS_2 is considered, polymer cannot penetrate inside the droplets and can interact with fullerene only at their interface. Therefore, the specific growth into nanoplatelets is very likely to occur at the interface, which could explain their peculiar 2D morphology.

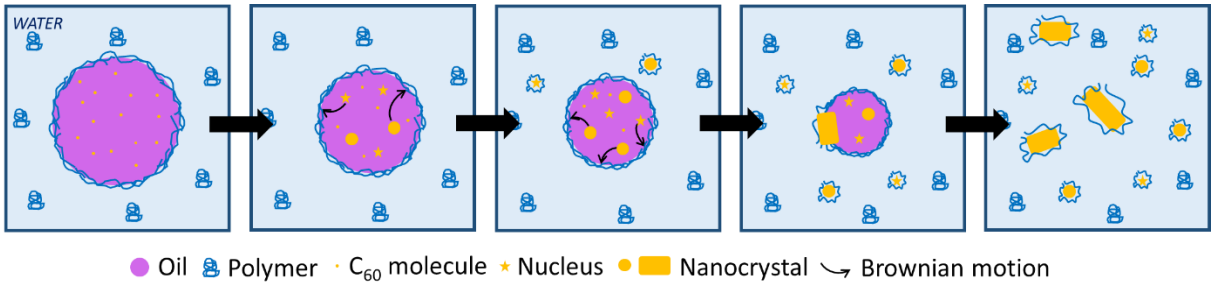

Scheme 1. Schematic overview of the mechanism of C_{60} particle formation and dispersion by the emulsification-evaporation method in the presence of the amphiphilic polymer.

This mechanism can explain why with increasing polymer concentration the yield increased and the particle size decreased. In order to obtain effective coverage of the particles, the polymer concentration relative to the C_{60} concentration should then be more important to consider than its absolute concentration. When plotting in **Figure 6a** the yield as a function of the relative concentration, defined as the molar ratio of 75C12 repeating units to C_{60} molecules, rather than as a function of the total concentration shown in **Figure S8b-c**, the results for various dispersions superimpose better. However, dispersions obtained with the polymer dissolved in chloroform still show an increase of the yield at lower relative polymer concentrations compared to samples in which polymer was initially dissolved in water. This is possibly due to the fact that the in the former case, the polymer is more readily available to bind to the particles. We indeed observed that the emulsions prepared with the polymer initially dissolved in chloroform were more stable than when the polymer was first dissolved

in water. In the former case, the polymer diffuses to the interface more easily. The decrease of the yield with increasing Φ_{org}> 25% (see Figure S12a) can also be explained by a decrease of the relative polymer concentration as the total amount of C_{60} in the organic phase increased and that of 75C12 in the aqueous phase decreased. However, this cannot explain the decrease of the yield for Φ_{org}< 25% (see **Figure S12b**). One possibility is that a small fraction of the solvent wets the glass walls and therefore does not allow a fraction of the fullerene to disperse. The effect of the polymer concentration on R_h also better superimposes when plotted as a function of the relative concentration, see **Figure 6b** vs. Figure 2b. It can explain why no significant decrease of R_h was found for dispersions made with method M5, because the relative polymer concentrations tested were not high enough. R_h levelled off with decreasing C_{pol} at the same relative concentration at which the yield started to decrease. This suggests that larger particles that were formed at lower polymer concentrations did not disperse well leading to a decrease of the yield.

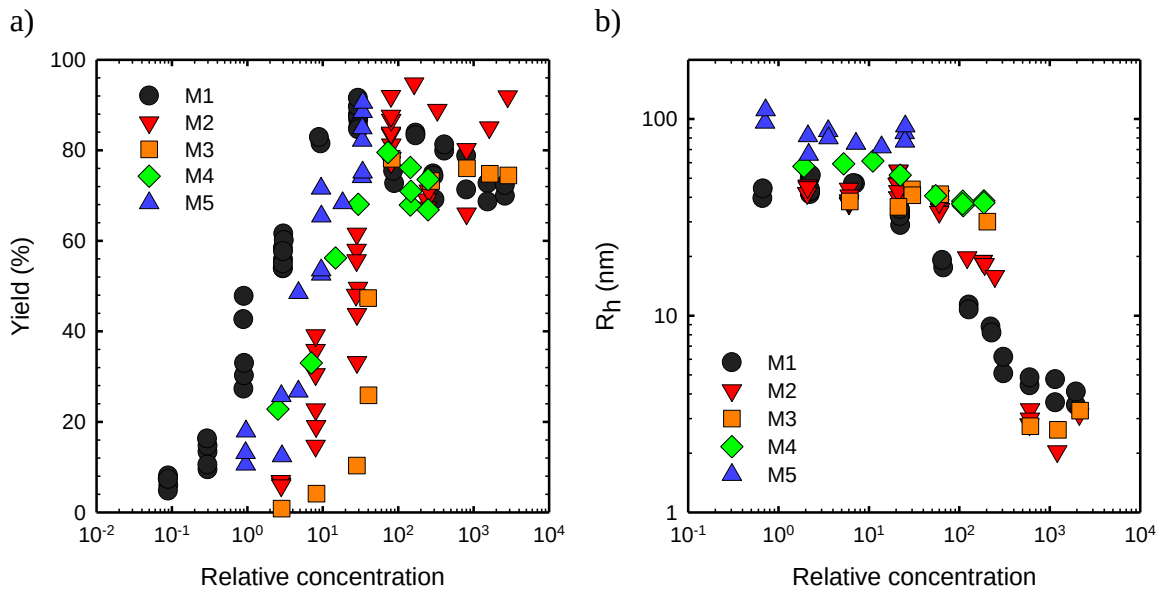

Figure 6. Dispersion yield (a) and R_h (b) as a function of the relative polymer concentration expressed as the molar ratio between polymer repeating units and C_{60} for dispersions produced with different methods as indicated in the figure.

The size of the particles at low relative polymer concentrations increased with increasing concentration of C_{60} dissolved in the organic phase. We speculate that growth was faster when more C_{60} was present so that the particles were larger before interaction with the polymer inhibited further growth.

The variety of the shape and the size dispersity of the C_{60} particles renders it difficult to interpret the observed relationships between R_h and R_g and that between R_h and M_w. Cryo-

TEM images showed that nanocrystals had formed in the shape of platelets when the dispersions were prepared with higher concentrations of fullerene. Various shapes of C_{60} nanocrystals have been reported in the literature so far.[49-53] Formation of C_{60} nanoplatelets displaying rectangular shapes similar to what was observed in this study was reported with aerosol. [52] However, in the latter study the higher contrast observed from in TEM may indicate that the platelets were thicker than the one we report on. Also, when they were tilted, they displayed a hexagonal geometry, which was not seen in the current investigation. In water, nanocrystals are typically obtained when C_{60} is precipitated from THF, which produces nanocrystals in the shape of parallelepipeds with sharp edges and high contrast in TEM.[28]
As far as we are aware, the particular round-edged rectangular platelet shape has not been reported in the literature and may be related to specific interactions with 75C12. As these nanocrystals are already dispersed in water, they are readily useable for potential applications. Further study is needed to elucidate the detailed structure of the nanoplatelets, their properties and the mechanism of their formation.

5. Conclusions

Aqueous colloidal dispersions of C_{60} nanoparticles have been produced using an emulsification-evaporation method in the presence of an amphiphilic cationic polymer. Its chemical structure has been chosen in order to promote, in water, interactions with fullerene C_{60} such as hydrophobic and π-π stacking ones. Furthermore, the amphiphilic and polyelectrolyte nature of the polymer was expected to achieve the stability of the fullerene nanoparticles through electrostatic repulsion combined with an increase of the viscosity of the aqueous phase upon increasing polymer concentration. The concentration of fullerene nanoparticles that can be dispersed in water went up to 8 g/L which is the highest value reported so far for emulsification-evaporation as well as other processes aiming at dispersing neat C_{60} into aqueous colloidal suspensions as evidenced from Table 2. Such a high value is explained both by the use of the polymer as well as the optimization of the processing parameters (type, concentration and amount of the organic phase together with polymer concentration). The latter also affect the morphology of the colloidal fullerene nanoparticles. The most concentrated dispersions showed indeed the formation of nanocrystals in the form of thin elongated platelets with lengths up to a few hundreds of nm. Such a 2D morphology is likely to occur by interfacial growth of the colloids thanks to specific interactions with the amphiphilic polymer. The fact that high amount of fullerene colloids can be produced in one step is valuable for in the future integrating them into hydrogels formed by the amphiphilic

polymer to form full carbon-based nanocomposite hydrogels[54] displaying combined functional properties of both components and mechanical reinforcement thanks to the strong interactions between the polymer and the fullerene nanoparticles. Lastly, self-assembled fullerene into 2D materials constitute an interesting class of materials for various application fields such as sensors, solar cells, drug delivery, as recently reviewed. [55]

Table 2. Concentration of C60 fullerene that can be dispersed in water with various processes and the assistance of various polymers.

Process	Stabilizer	Fullerene concentration (g/L)	Ref.
Emulsification-evaporation	Triton X-100	20.10^{-3}	[51]
Emulsification-evaporation	None	1.4	[31, 32]
Emulsification-evaporation	75C12	8.0	Present work
Nanoprecipitation	Cholesteryl-bearing pullulan	0.6	[29]
Drying/re-dispersion	Peptide	1.3	[30]

Supporting Information

Supporting Information is available online.

Author Contributions

Théo Merland: Investigation, Writing – original draft; Clément Drou: Investigation; Stéphanie Legoupy: Writing – review & editing; Lazhar Benyahia: Writing – review & editing; Marc Schmutz: Investigation, Writing – original draft; Taco Nicolai: Supervision, Writing – review & editing; Christophe Chassenieux: Conceptualization, Supervision, Writing – original draft.

Conflicts of Interest

The authors declare no conflict of interest.

Acknowledgements

The authors acknowledge the support of Le Mans Université in the frame of the regional SPEED (Smart sustainable PolymErs and procEss Development) program.

References

[1] J.W. Arbogast, A.P. Darmanyan, C.S. Foote, F. Diederich, R. Whetten, Y. Rubin, M.M. Alvarez, S.J. Anz, Photophysical properties of sixty atom carbon molecule (C60), The Journal of Physical Chemistry 95(1) (1991) 11-12.
[2] M. Di Giosia, F. Nicolini, L. Ferrazzano, A. Soldà, F. Valle, A. Cantelli, T.D. Marforio, A. Bottoni, F. Zerbetto, M. Montalti, S. Rapino, A. Tolomelli, M. Calvaresi, Stable and Biocompatible Monodispersion of C60 in Water by Peptides, Bioconjugate Chemistry 30(3) (2019) 808-814.
[3] D.M. Guldi, Capped Fullerenes: Stabilization of Water-Soluble Fullerene Monomers As Studied by Flash Photolysis and Pulse Radiolysis, The Journal of Physical Chemistry A 101(21) (1997) 3895-3900.
[4] Y. Iwamoto, Y. Yamakoshi, A highly water-soluble C 60–NVP copolymer: a potential material for photodynamic therapy, Chemical communications (46) (2006) 4805-4807.
[5] D.Y. Lyon, L.K. Adams, J.C. Falkner, P.J.J. Alvarez, Antibacterial Activity of Fullerene Water Suspensions : Effects of Preparation Method and Particle Size, Environmental Science & Technology 40(14) (2006) 4360-4366.
[6] Z. Markovic, B. Todorovic-Markovic, D. Kleut, N. Nikolic, S. Vranjes-Djuric, M. Misirkic, L. Vucicevic, K. Janjetovic, A. Isakovic, L. Harhaji, B. Babic-Stojic, M. Dramicanin, V. Trajkovic, The mechanism of cell-damaging reactive oxygen generation by colloidal fullerenes, Biomaterials 28(36) (2007) 5437-5448.
[7] E. Nakamura, H. Tokuyama, S. Yamago, T. Shiraki, Y. Sugiura, Biological Activity of Water-Soluble Fullerenes. Structural Dependence of DNA Cleavage, Cytotoxicity, and Enzyme Inhibitory Activities Including HIV-Protease Inhibition, Bulletin of the Chemical Society of Japan 69(8) (1996) 2143-2151.
[8] Y. Tabata, Y. Murakami, Y. Ikada, Photodynamic Effect of Polyethylene Glycol–modified Fullerene on Tumor, Japanese Journal of Cancer Research 88(11) (1997) 1108-1116.
[9] D.Y. Lyon, P.J.J. Alvarez, Fullerene Water Suspension (nC(60)) Exerts Antibacterial Effects via ROS-Independent Protein Oxidation, Environmental Science & Technology 42(21) (2008) 8127-8132.
[10] T. Aernouts, T. Aleksandrov, C. Girotto, J. Genoe, J. Poortmans, Polymer based organic solar cells using ink-jet printed active layers, Applied Physics Letters 92(3) (2008) 033306.
[11] T.R. Andersen, T.T. Larsen-Olsen, B. Andreasen, A.P.L. Böttiger, J.E. Carlé, M. Helgesen, E. Bundgaard, K. Norrman, J.W. Andreasen, M. Jørgensen, F.C. Krebs, Aqueous Processing of Low-Band-Gap Polymer Solar Cells Using Roll-to-Roll Methods, ACS Nano 5(5) (2011) 4188-4196.
[12] S. Zappia, G. Scavia, A.M. Ferretti, U. Giovanella, V. Vohra, S. Destri, Water-Processable Amphiphilic Low Band Gap Block Copolymer:Fullerene Blend Nanoparticles as Alternative Sustainable Approach for Organic Solar Cells, Advanced Sustainable Systems 2(3) (2018).
[13] R.S. Ruoff, D.S. Tse, R. Malhotra, D.C. Lorents, Solubility of fullerene (C60) in a variety of solvents, The Journal of Physical Chemistry 97(13) (1993) 3379-3383.

[14] J.A. Brant, J. Labille, C.O. Robichaud, M. Wiesner, Fullerol cluster formation in aqueous solutions: Implications for environmental release, Journal of Colloid and Interface Science 314(1) (2007) 281-288.
[15] L.Y. Chiang, J.W. Swirczewski, C.S. Hsu, S.K. Chowdhury, S. Cameron, K. Creegan, Multi-hydroxy additions onto C60 fullerene molecules, Journal of the Chemical Society, Chemical Communications (24) (1992) 1791-1793.
[16] I. Lamparth, A. Hirsch, Water-soluble malonic acid derivatives of C60 with a defined three-dimensional structure, Journal of the Chemical Society, Chemical Communications (14) (1994) 1727-1728.
[17] K.D. Pickering, M.R. Wiesner, Fullerol-Sensitized Production of Reactive Oxygen Species in Aqueous Solution, Environmental Science & Technology 39(5) (2005) 1359-1365.
[18] B. Vileno, P.R. Marcoux, M. Lekka, A. Sienkiewicz, T. Fehér, L. Forró, Spectroscopic and Photophysical Properties of a Highly Derivatized C60 Fullerol, Advanced Functional Materials 16(1) (2006) 120-128.
[19] M. Hiroto, S. Masaharu, S. Takamasa, N. Naotoshi, Synthesis, Aggregate Structure and Electrochemical Properties of a Water-Soluble Fullerene-Bearing Ammonium Amphiphile, Chemistry Letters 28(8) (1999) 815-816.
[20] S. Masaya, N. Noriaki, T. Motoki, H.U. E., I. Hiroyuki, N. Eiichi, Z. Shui-Quin, C. Benjamin, Pentaorgano[60]fullerene R5C60−. A Water Soluble Hydrocarbon Anion, Chemistry Letters 29(9) (2000) 1098-1099.
[21] K. Kokubo, K. Matsubayashi, H. Tategaki, H. Takada, T. Oshima, Facile synthesis of highly water-soluble fullerenes more than half-covered by hydroxyl groups, Acs Nano 2(2) (2008) 327-333.
[22] K.N. Semenov, N.A. Charykov, V.N. Keskinov, Fullerenol Synthesis and Identification. Properties of the Fullerenol Water Solutions, Journal of Chemical & Engineering Data 56(2) (2011) 230-239.
[23] M.T. Dang, L. Hirsch, G. Wantz, P3HT:PCBM, Best Seller in Polymer Photovoltaic Research, Advanced Materials 23(31) (2011) 3597-3602.
[24] M.E. Hilburn, B.S. Murdianti, R.D. Maples, J.S. Williams, J.T. Damron, S.I. Kuriyavar, K.D. Ausman, Synthesizing aqueous fullerene colloidal suspensions by new solvent-exchange methods, Colloids and Surfaces a-Physicochemical and Engineering Aspects 401 (2012) 48-53.
[25] J. Brant, H. Lecoanet, M.R. Wiesner, Aggregation and Deposition Characteristics of Fullerene Nanoparticles in Aqueous Systems, Journal of Nanoparticle Research 7(4) (2005) 545-553.
[26] S. Andreev, D. Purgina, E. Bashkatova, A. Garshev, A. Maerle, I. Andreev, N. Osipova, N. Shershakova, M. Khaitov, Study of Fullerene Aqueous Dispersion Prepared by Novel Dialysis Method: Simple Way to Fullerene Aqueous Solution, Fullerenes Nanotubes and Carbon Nanostructures 23(9) (2015) 792-800.
[27] S. Deguchi, R.G. Alargova, K. Tsujii, Stable Dispersions of Fullerenes, C60 and C70, in Water. Preparation and Characterization, Langmuir 17(19) (2001) 6013-6017.
[28] J.D. Fortner, D.Y. Lyon, C.M. Sayes, A.M. Boyd, J.C. Falkner, E.M. Hotze, L.B. Alemany, Y.J. Tao, W. Guo, K.D. Ausman, V.L. Colvin, J.B. Hughes, C-60 in water: Nanocrystal formation and microbial response, Environmental Science & Technology 39(11) (2005) 4307-4316.
[29] L. Douglas, N. Markus, M. Mutsuo, S. Junzo, Complexation of C60 Fullerene with Cholesteryl Group-Bearing Pullulan in Aqueous Medium, Chemistry Letters 29(1) (2000) 64-65.
[30] S. Bartocci, D. Mazzier, A. Moretto, M. Mba, A peptide topological template for the dispersion of 60 fullerene in water, Organic & Biomolecular Chemistry 13(2) (2015) 348-352.

[31] G.V. Andrievsky, V.K. Klochkov, A.B. Bordyuh, G.I. Dovbeshko, Comparative analysis of two aqueous-colloidal solutions of C60 fullerene with help of FTIR reflectance and UV-Vis spectroscopy, Chemical Physics Letters 364(1) (2002) 8-17.
[32] G.V. Andrievsky, V.K. Klochkov, E.L. Karyakina, N.O. McHedlov-Petrossyan, Studies of aqueous colloidal solutions of fullerene C60 by electron microscopy, Chemical Physics Letters 300(3) (1999) 392-396.
[33] F. Almyahi, T.R. Andersen, N. Cooling, N.P. Holmes, A. Fahy, M.G. Barr, D. Kilcoyne, W. Belcher, P.C. Dastoor, Optimization, characterization and upscaling of aqueous solar nanoparticle inks for organic photovoltaics using low-cost donor: acceptor blend, Organic Electronics 52 (2018) 71-78.
[34] N.P. Holmes, M. Marks, P. Kumar, R. Kroon, M.G. Barr, N. Nicolaidis, K. Feron, A. Pivrikas, A. Fahy, A.D.d.Z. Mendaza, A.L.D. Kilcoyne, C. Müller, X. Zhou, M.R. Andersson, P.C. Dastoor, W.J. Belcher, Nano-pathways: Bridging the divide between water-processable nanoparticulate and bulk heterojunction organic photovoltaics, Nano Energy 19 (2016) 495-510.
[35] T. Andersson, K. Nilsson, M. Sundahl, G. Westman, O. Wennerström, C60 embedded in γ-cyclodextrin: a water-soluble fullerene, Journal of the Chemical Society, Chemical Communications (8) (1992) 604-606.
[36] J. Lee, J.D. Fortner, J.B. Hughes, J.-H. Kim, Photochemical Production of Reactive Oxygen Species by C60 in the Aqueous Phase During UV Irradiation, Environmental Science & Technology 41(7) (2007) 2529-2535.
[37] Y.N. Yamakoshi, T. Yagami, K. Fukuhara, S. Sueyoshi, N. Miyata, Solubilization of fullerenes into water with polyvinylpyrrolidone applicable to biological tests, Journal of the Chemical Society, Chemical Communications (4) (1994) 517-518.
[38] C.N. Allen, N. Lequeux, C. Chassenieux, G. Tessier, B. Dubertret, Optical Analysis of Beads Encoded with Quantum Dots Coated with a Cationic Polymer, Advanced Materials 19(24) (2007) 4420-4425.
[39] T. Hirai, T. Watanabe, I. Komasawa, Preparation of Semiconductor Nanoparticle−Polymer Composites by Direct Reverse Micelle Polymerization Using Polymerizable Surfactants, The Journal of Physical Chemistry B 104(38) (2000) 8962-8966.
[40] H. Zhang, Z. Cui, Y. Wang, K. Zhang, X. Ji, C. Lü, B. Yang, M. Gao, From Water-Soluble CdTe Nanocrystals to Fluorescent Nanocrystal–Polymer Transparent Composites Using Polymerizable Surfactants, Advanced Materials 15(10) (2003) 777-780.
[41] M. Save, M. Manguian, C. Chassenieux, B. Charleux, Synthesis by RAFT of Amphiphilic Block and Comblike Cationic Copolymers and Their Use in Emulsion Polymerization for the Electrosteric Stabilization of Latexes, Macromolecules 38(2) (2005) 280-289.
[42] F. Dutertre, C. Gaillard, C. Chassenieux, T. Nicolai, Branched Wormlike Micelles Formed by Self-Assembled Comblike Amphiphilic Copolyelectrolytes, Macromolecules 48(20) (2015) 7604-7612.
[43] C. Limouzin-Morel, F. Dutertre, W. Moussa, C. Gaillard, I. Iliopoulos, D. Bendejacq, T. Nicolai, C. Chassenieux, One and two dimensional self-assembly of comb-like amphiphilic copolyelectrolytes in aqueous solution, Soft Matter 9(37) (2013) 8931-8937.
[44] J. Jakeš, Regularized Positive Exponential Sum (REPES) Program - A Way of Inverting Laplace Transform Data Obtained by Dynamic Light Scattering, Collect. Czech. Chem. Commun.
60 (1995) 1781-1797.
[45] G.V. Andrievsky, M.V. Kosevich, O.M. Vovk, V.S. Shelkovsky, L.A. Vashchenko, On the production of an aqueous colloidal solution of fullerenes, Journal of the Chemical Society, Chemical Communications (12) (1995) 1281-1282.

[46] P. Scharff, K. Risch, L. Carta-Abelmann, I.M. Dmytruk, M.M. Bilyi, O.A. Golub, A.V. Khavryuchenko, E.V. Buzaneva, V.L. Aksenov, M.V. Avdeev, Y.I. Prylutskyy, S.S. Durov, Structure of C60 fullerene in water : spectroscopic data, Carbon 42(5) (2004) 1203-1206.
[47] Z. Chen, P. Westerhoff, P. Herckes, Quantification of C60 fullerene concentrations in water, Environmental Toxicology and Chemistry 27(9) (2008) 1852-1859.
[48] F. Dutertre, L. Benyahia, C. Chassenieux, T. Nicolai, Dynamic Mechanical Properties of Networks of Wormlike Micelles Formed by Self-Assembled Comblike Amphiphilic Copolyelectrolytes, Macromolecules 49(18) (2016) 7045-7053.
[49] K. Kobayashi, M. Tachibana, K. Kojima, Photo-assisted growth of C60 nanowhiskers from solution, Journal of Crystal Growth 274(3) (2005) 617-621.
[50] A. Masuhara, Z. Tan, H. Kasai, H. Nakanishi, H. Oikawa, Fullerene Fine Crystals with Unique Shapes and Controlled Size, Japanese Journal of Applied Physics 48(5) (2009) 050206.
[51] C. Park, H.J. Song, H.C. Choi, The critical effect of solvent geometry on the determination of fullerene (C60) self-assembly into dot, wire and disk structures, Chemical Communications (32) (2009) 4803-4805.
[52] B. Pauwels, D. Bernaerts, S. Amelinckx, G. Van Tendeloo, J. Joutsensaari, E.I. Kauppinen, Multiply twinned C60 and C70 nanoparticles, Journal of Crystal Growth 200(1) (1999) 126-136.
[53] Z. Tan, A. Masuhara, H. Kasai, H. Nakanishi, H. Oikawa, Multibranched C60Micro/Nanocrystals Fabricated by Reprecipitation Method, Japanese Journal of Applied Physics 47(2) (2008) 1426-1428.
[54] K. Sugikawa, Y. Inoue, K. Kozawa, A. Ikeda, Introduction of Fullerenes into Hydrogels via Formation of Fullerene Nanoparticles, ChemNanoMat 4(7) (2018) 682-687.
[55] A.V. Baskar, M.R. Benzigar, S.N. Talapaneni, G. Singh, A.S. Karakoti, J. Yi, A.a.H. Al-Muhtaseb, K. Ariga, P.M. Ajayan, A. Vinu, Self-Assembled Fullerene Nanostructures: Synthesis and Applications, Advanced Functional Materials 32(6) (2022) 2106924.

Figure captions

Figure 1. Chemical structure of the amphiphilic copolymer 75C12, 75 stands for the relative molar ratio in % of cationic moieties which contain dodecyl (C12) side chains.

Figure 2. Concentration (a) and hydrodynamic radius (b) of fullerene nanoparticles dispersed in water as a function of the polymer concentration and with different methods of dispersion as indicated in the legend of the figure.

Figure 3. Concentration of fullerene particles dispersed in water (a) and their hydrodynamic radius (b) as function of the volume fraction of CS_2 for methods M6 and M7. The polymer concentration in the aqueous phase is indicated in the figure.

Figure 4. Weight average molar mass of fullerene particles as a function of their hydrodynamic radius.

Figure 5. Cryo-TEM pictures for samples a) M5 (C_{pol}=10 g/L, Φ_{org}=25%), b) M7 (C_{pol}=35 g/L, Φ_{org}=75%), c) M6 (C_{pol}=35 g/L, Φ_{org}=10%) and d) M4 (C_{pol}=10 g/L, Φ_{org}=25%). Short white arrows indicate polymeric worm-like micelles; the long white arrow shows Carbon-

Formvar lacey supporting film; short black arrows show small isotropic fullerene particles; the long black arrow shows a fullerene nanoplatelet.

Scheme 1. Schematic overview of the mechanism of C_{60} particle formation and dispersion by the emulsification-evaporation method in the presence of the amphiphilic polymer.

Figure 6. Dispersion yield (a) and R_h (b) as a function of the relative polymer concentration expressed as the molar ratio between polymer repeating units and C_{60} for dispersions produced with different methods as indicated in the figure.

Tables

Table 1. Summary of the various conditions used to disperse C_{60} in water.

Method	Organic solvent	Polymer concentration[a)] (g/L) / solvent	C_{60} concentration in organic phase (g/L)	Volume fraction of organic phase
M1	$CHCl_3$	1.10^{-3} to 35 / $CHCl_3$	0.09[b]	25%
M2	$CHCl_3$	35.10^{-3} to 35 / H_2O	0.09[b]	25%
M3	CS_2	35.10^{-3} to 35 / H_2O	0.09	25%
M4	CS_2	0.35 to 35 / H_2O	1	25%
M5	CS_2	1 to 35 / H_2O	7.6[b]	25%
M6	CS_2	35 / H_2O	7.6[b]	10 to 75%
M7	CS_2	10 / H_2O	7.6[b]	10 to 75%

[a)] Final concentration in water after evaporation of the organic solvent; [b)] saturation concentration for C_{60} fullerene in the organic phase.

Table 2. Concentration of C60 fullerene that can be dispersed in water with various processes and the assistance of various polymers.

Process	Stabilizer	Fullerene concentration (g/L)	Ref.
Emulsification-evaporation	Triton X-100	20.10^{-3}	52
Emulsification-evaporation	None	1.4	32,33
Emulsification-evaporation	75C12	8.0	Present work
Nanoprecipitation	Cholesteryl-bearing pullulan	0.6	30
Drying/re-dispersion	Peptide	1.3	31

Supporting Information for
Self-Assembly in water of C_{60} fullerene into isotropic nanoparticles or nanoplatelets mediated by a cationic amphiphilic polymer

Théo Merland[a], Clément Drou[b], Stéphanie Legoupy[b], Lazhar Benyahia[a], Marc Schmutz[c], Taco Nicolai[a], Christophe Chassenieux[a]*

[a]Institut des Molécules et Matériaux du Mans, UMR CNRS 6283, Le Mans Université, Avenue Olivier Messiaen, 72085 Le Mans Cedex 9, France.

[b]Univ Angers, CNRS, MOLTECH-ANJOU, F-49000 Angers, France.

[c]Institut Charles Sadron, UPR CNRS 22, 23 Rue du Loess, 67034 Strasbourg Cedex, France.

*Corresponding Author : Christophe Chassenieux, E-Mail: christophe.chassenieux@univ-lemans.fr

Emulsions macro- and microstructure characterization.

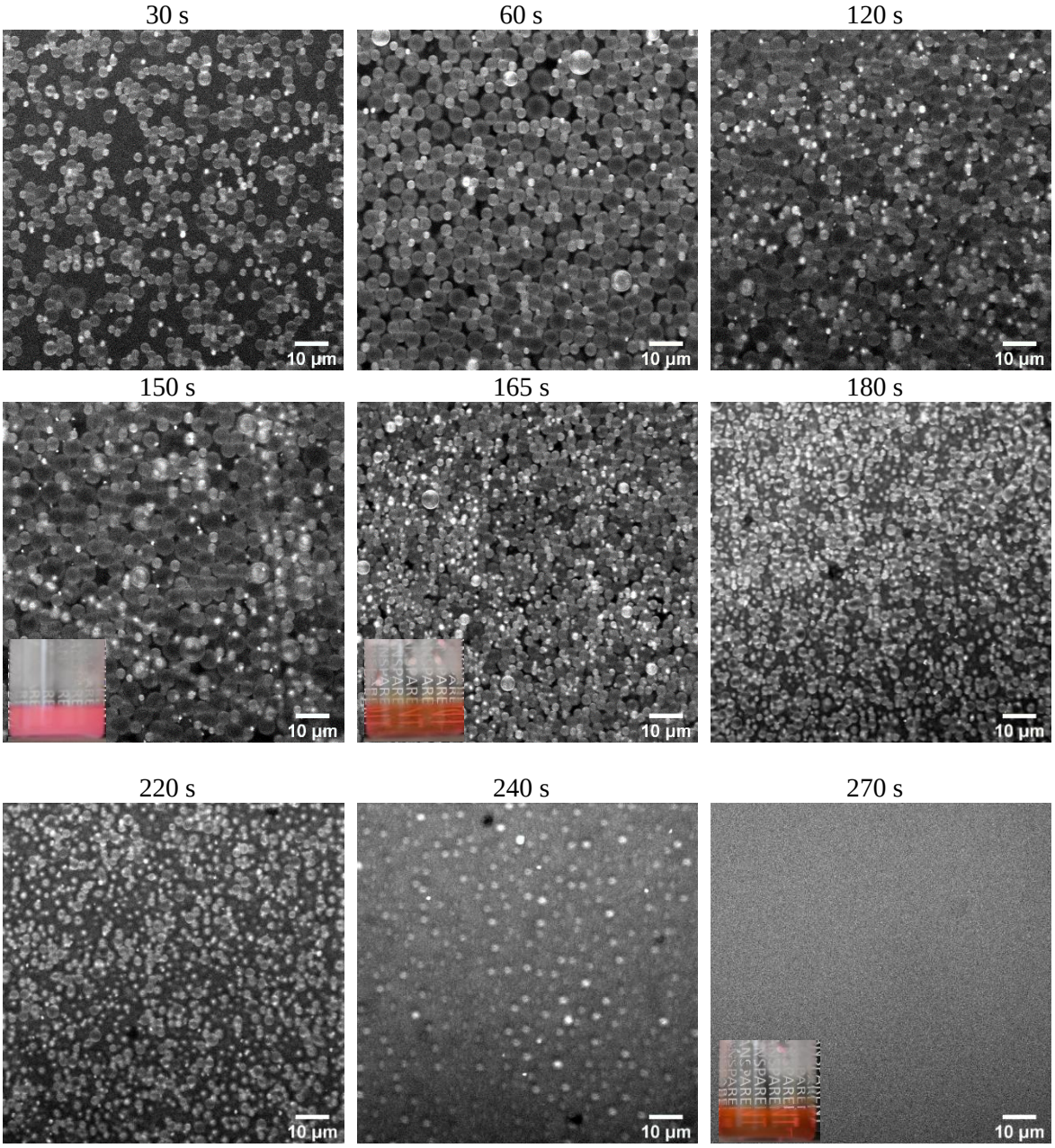

Figure S1. Confocal images of CS_2-in-water emulsions with C_{pol}=1 g/L and Φ_{org}=10% at different sonications times indicated above the pictures. Macroscopic pictures of the emulsions are in insert.

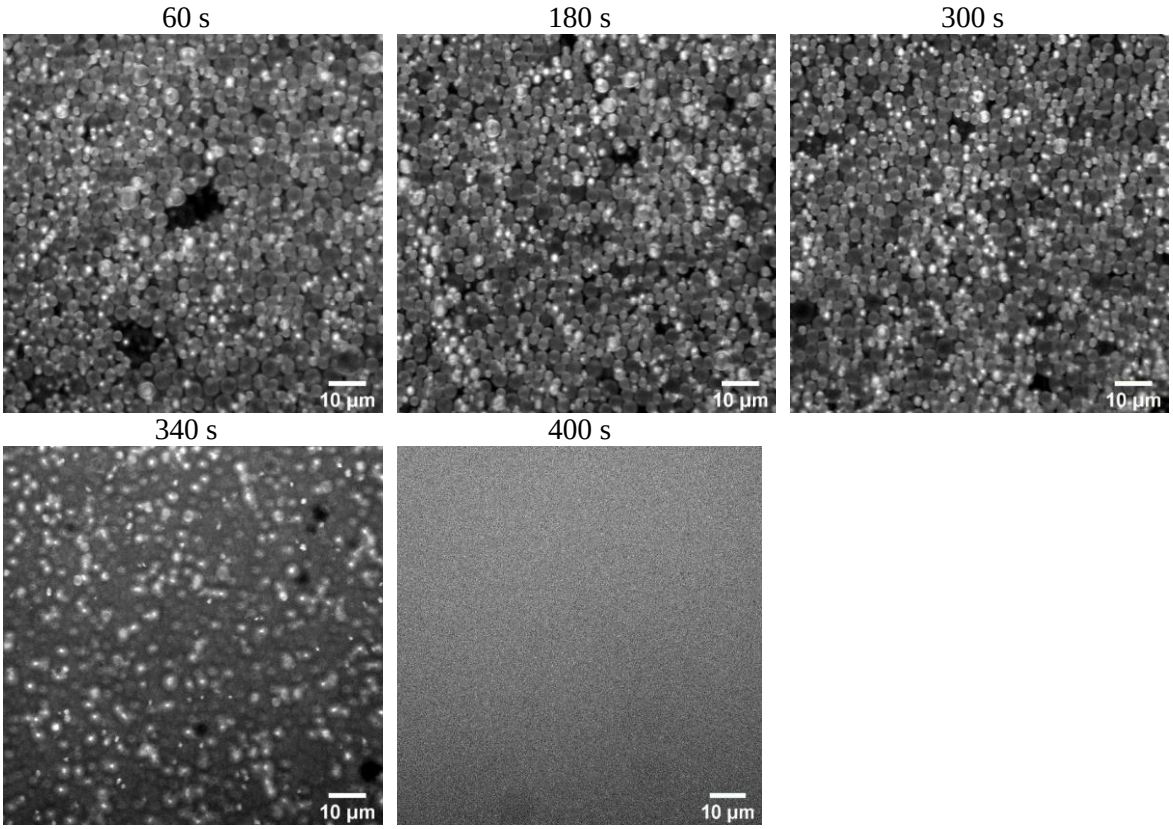

Figure S2. Confocal images of CS_2-in-water emulsions with C_{pol}=1 g/L and Φ_{org}=25% at different sonications times indicated above the pictures.

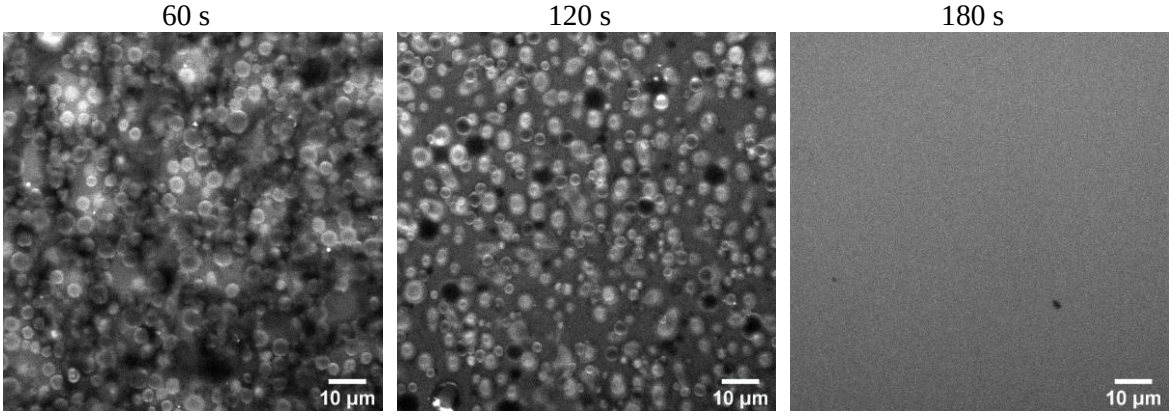

Figure S3. Confocal images of CS_2-in-water emulsions with C_{pol}=35 g/L and Φ_{org}=10% at different sonications times indicated above the pictures.

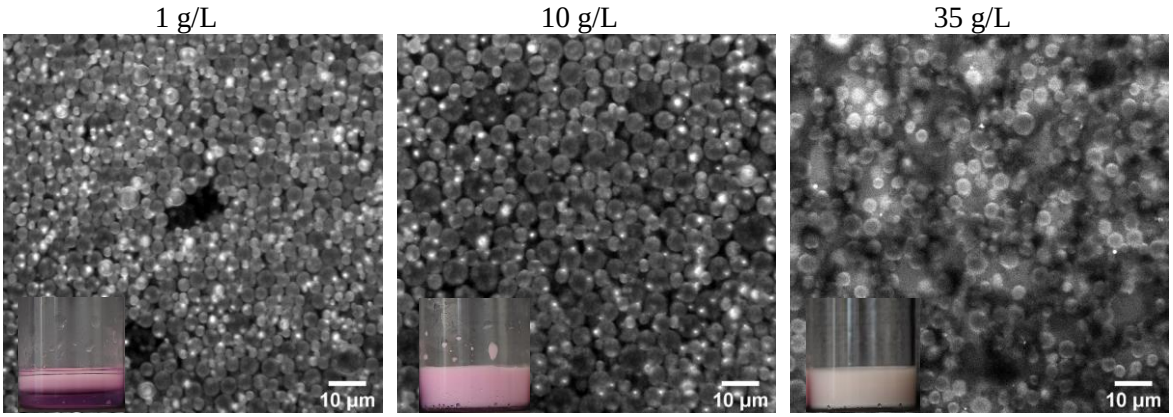

Figure S4. Confocal images of CS_2-in-water emulsions with various C_{pol} and Φ_{org}=10% after 1 minute of continuous sonication. Macroscopic pictures of the emulsions are in insert.

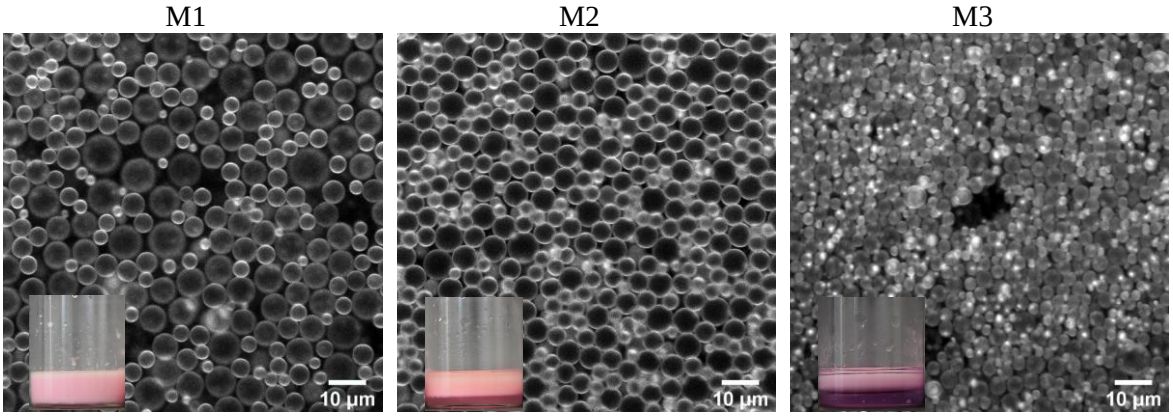

Figure S5. Confocal images of M1-2-3 emulsions with C_{pol}=1 g/L and Φ_{org}=10% after 1 minute of continuous sonication. Macroscopic pictures of the emulsions are in insert.

Pictures of samples.

Figure S6. From left to right, colloidal suspensions with C_{full} = 1 mg/L (without polymer), 25 mg/L (M2, C_{pol}=0.35 g/L), 0.26 g/L (M4, C_{pol}=20 g/L) and 1.6 g/L (M5, C_{pol}=10 g/L).

UV-visible spectroscopy.

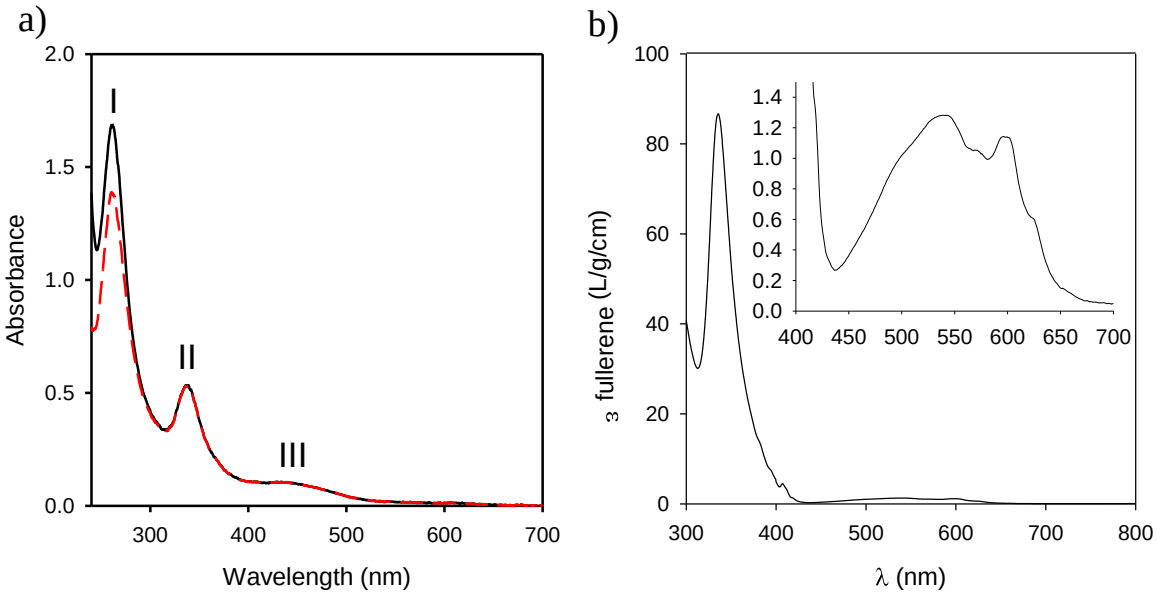

Figure S7. a) Absorption spectrum of an aqueous C_{60} dispersion obtained from M1 with 1 g/L 75C12 before (black solid line) and after subtraction of the contribution of 75C12 (red dashed line). b) Absorption coefficient of C_{60} in toluene. Insert is a magnification of visible light region.

Concentration and yield of dispersion for C_{60} in water.

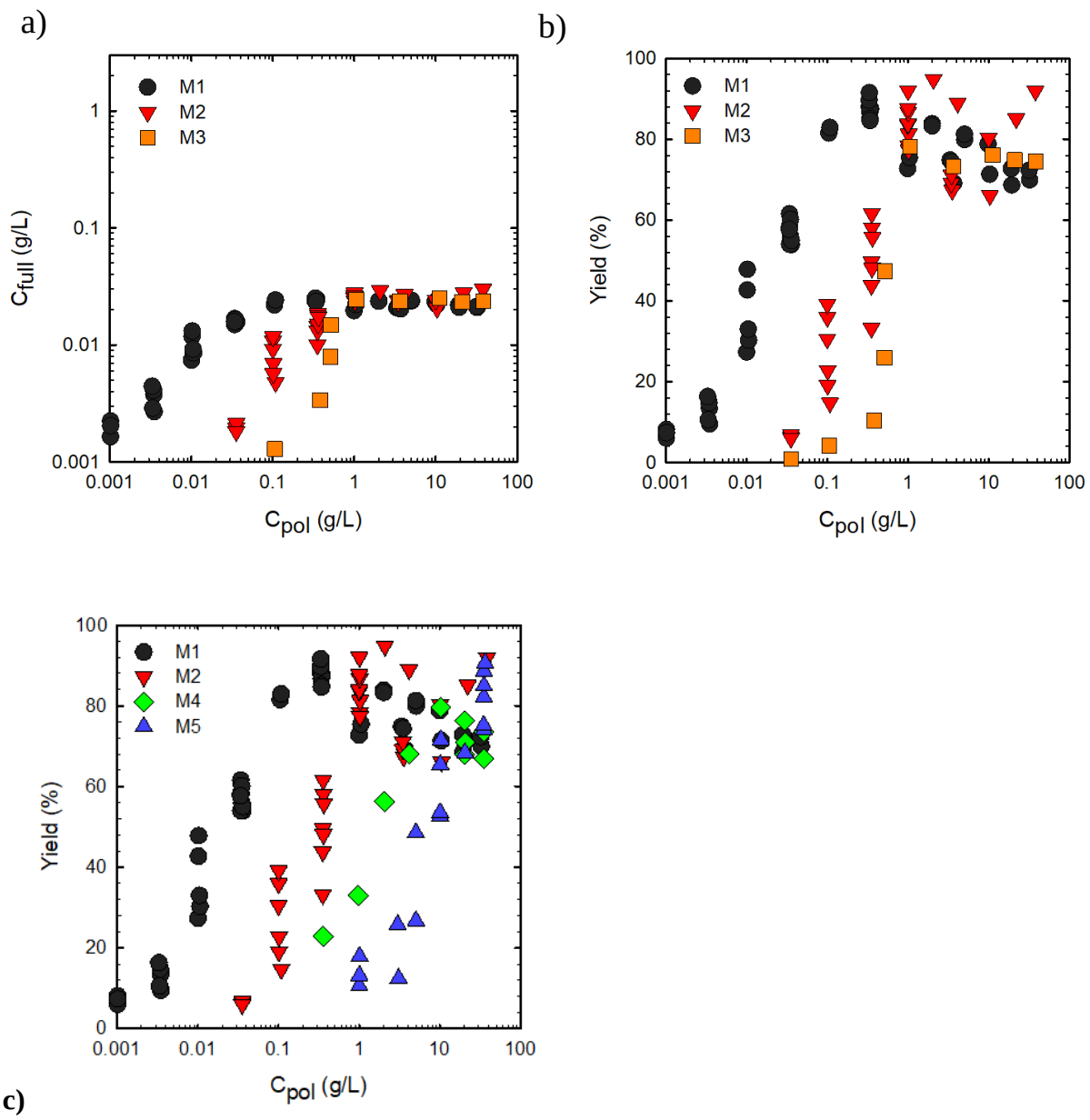

Figure S8. Concentration (a) and yield (b-c) of fullerene dispersed in water as a function of the polymer concentration for fullerene nanoparticles prepared with methods M1-3, results are also shown for methods M4 and M5 on a separated figure for the sake of clarity

Differential refractometry.

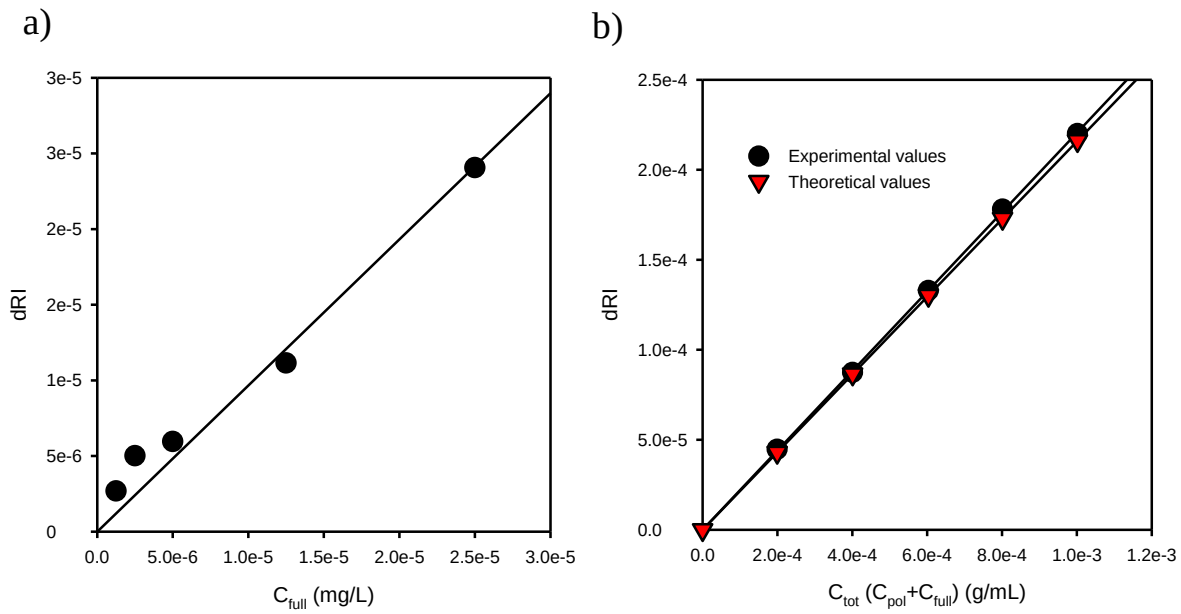

Figure S9. Concentration-dependence of refractive index (dRI) for samples prepared with C_{pol}= a) 0 and b) 35 g/L.

Structure of the nanoparticles.

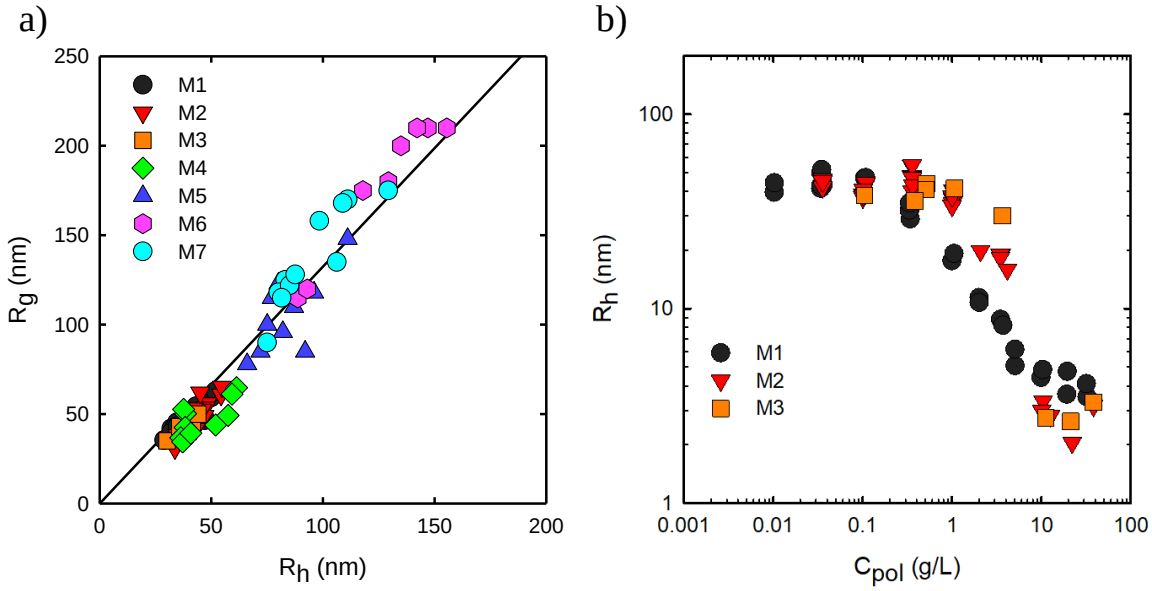

Figure S10. a) Gyration radius as a function of hydrodynamic radius. b) Hydrodynamic radius as a function of polymer concentration for methods M1-3.

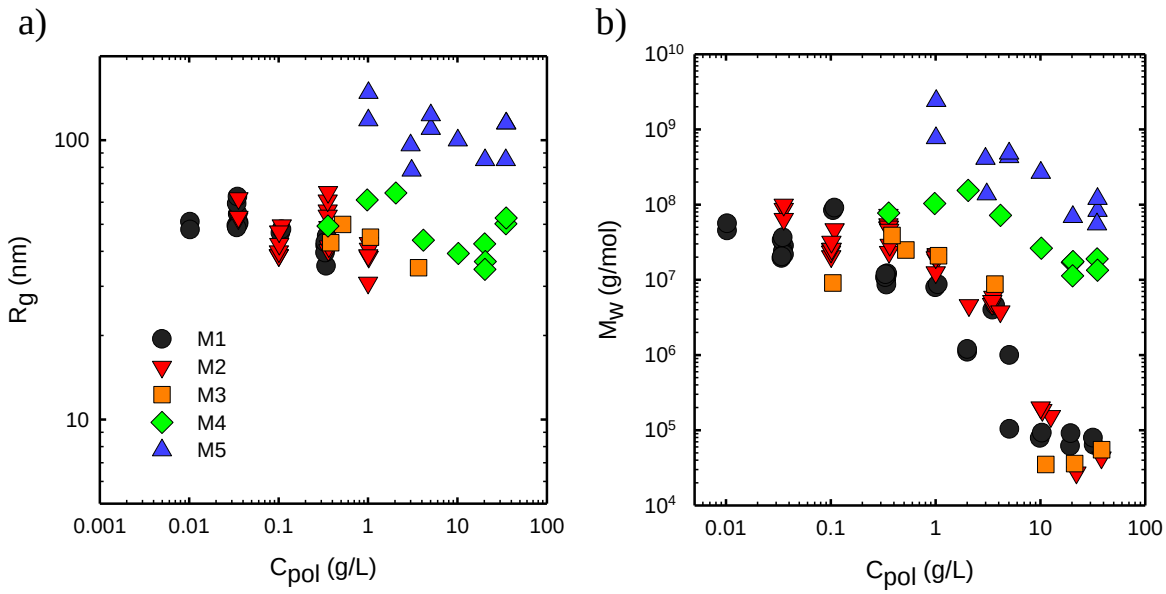

Figure S11. a) Gyration radius and b) Weight average molar mass of M1-5 samples as determined by SLS.

Influence of volumic fraction.

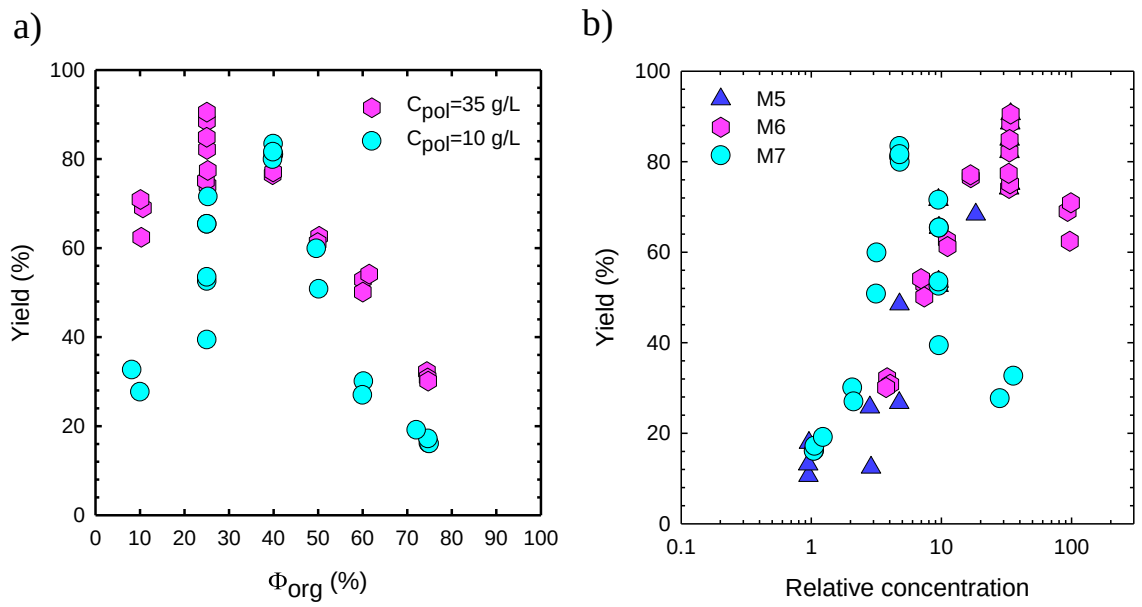

Figure S12. Dispersion yield as a function of a) volumic fraction of organic phase in the initial emulsions and b) relative concentration of 75C12 with respect to C_{60} for M5-7 samples. Polymer concentrations are indicated in legend.

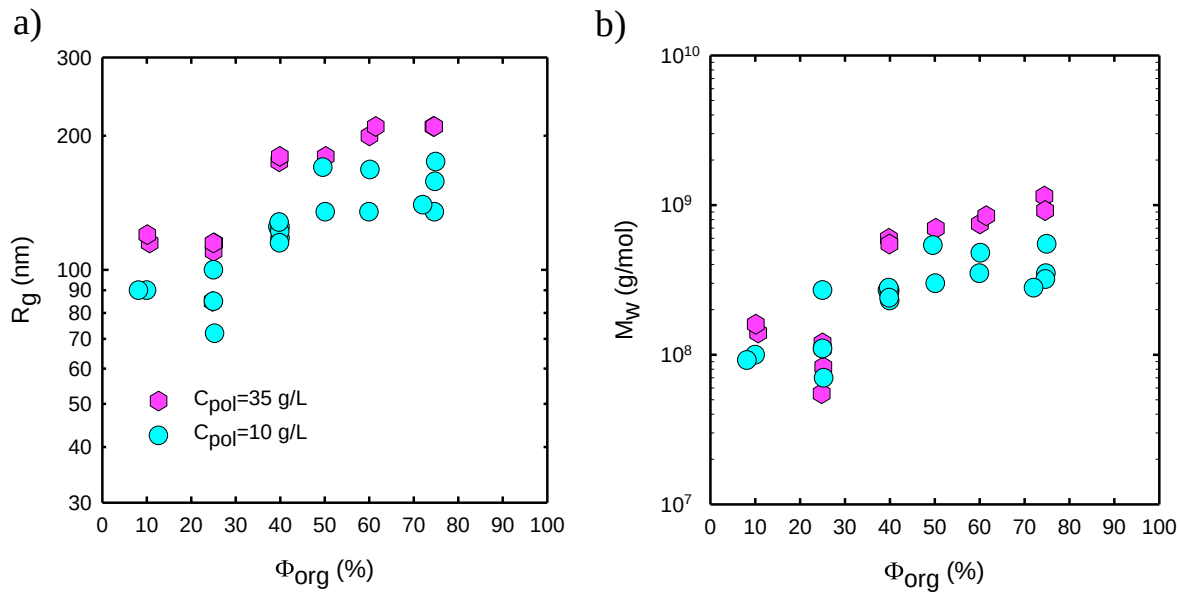

Figure S13. a) Gyration radius and b) Weight average molar mass of M6-7 samples with various volumic fractions of organic phase in the initial emulsions as determined by SLS. Polymer concentrations are indicated in legend.

Stability.

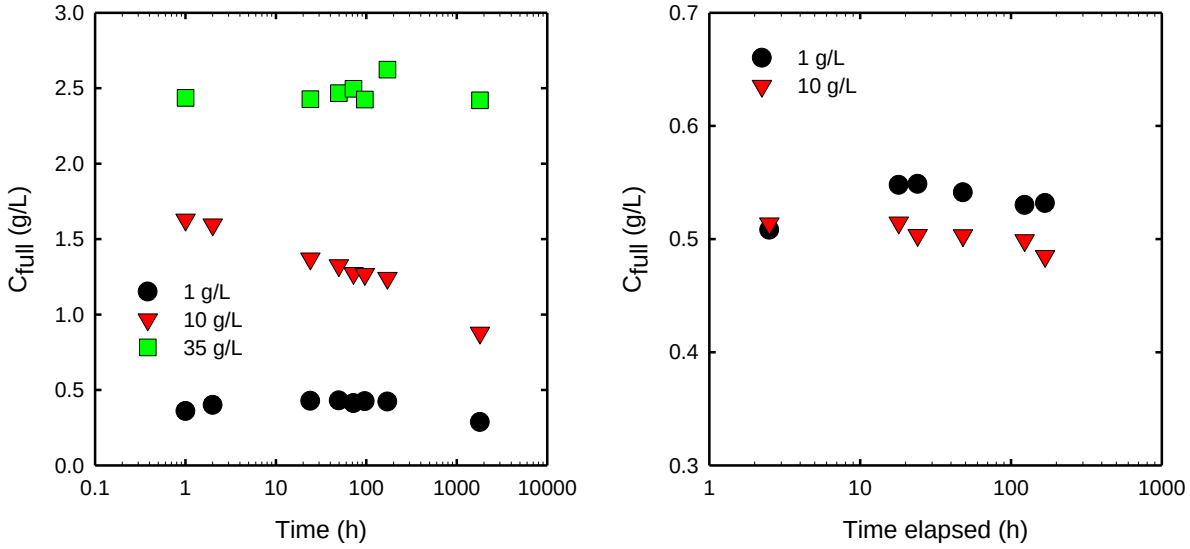

Figure S14. Stability over time of M5 samples a) with various C_{pol} as indicated in the legend. and b) for sample with C_{pol}=10 g/L which was diluted 3 times with a 10 g/L polymer solution to keep C_{pol} constant.

Polydispersity of the nanoparticles

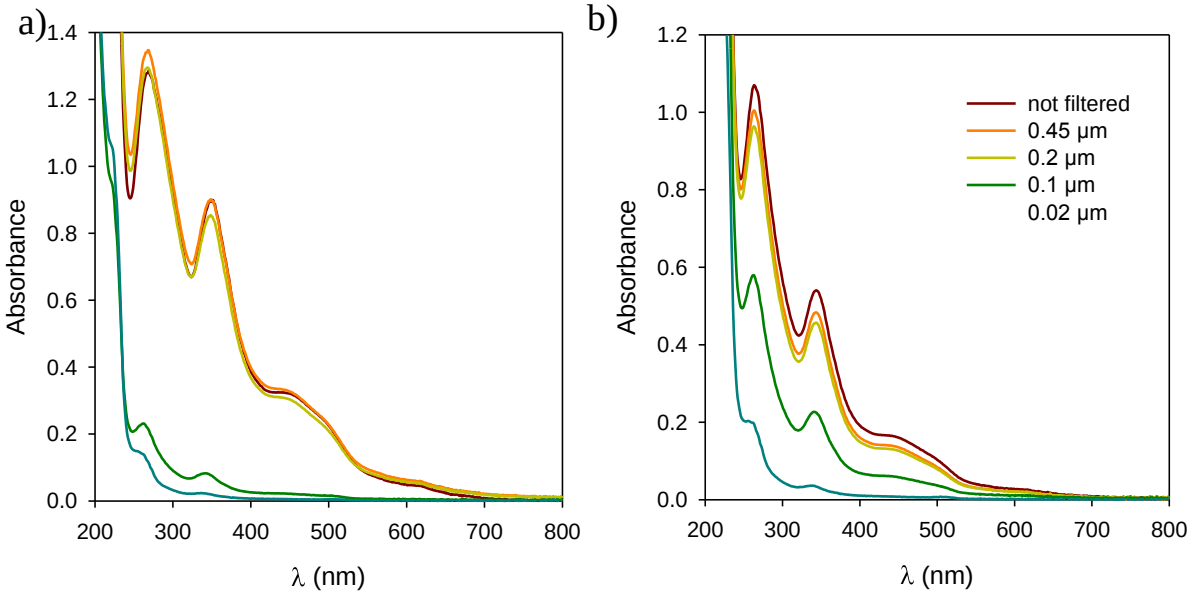

Figure S15. UV-visible absorption spectra of diluted M5 samples (C_{pol} = a) 10 g/L and b) 35 g/L) before and after filtration over various pore sizes indicated in legend.

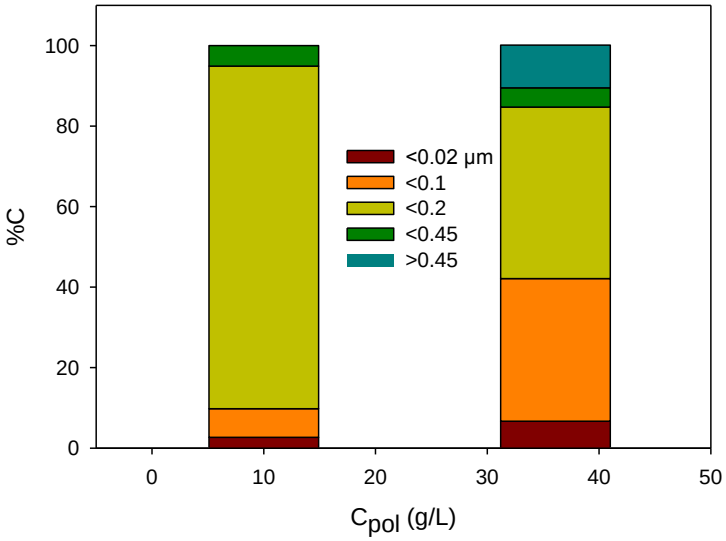

Figure S16. Percentage of particles concentration after filtration over various porosities indicated in legend for two M5 samples with C_{pol}=10 and 35 g/L.

TEM pictures.

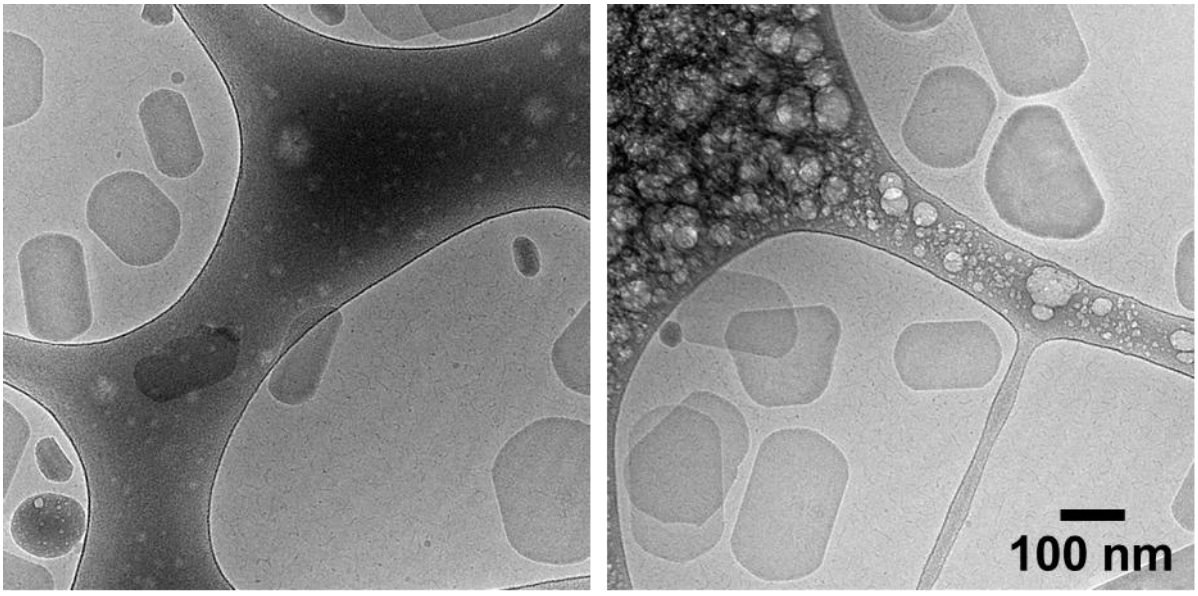

Figure S17. Cryo-TEM pictures of an M5 sample (C_{pol}=10 g/L, Φ_{org}=25%).

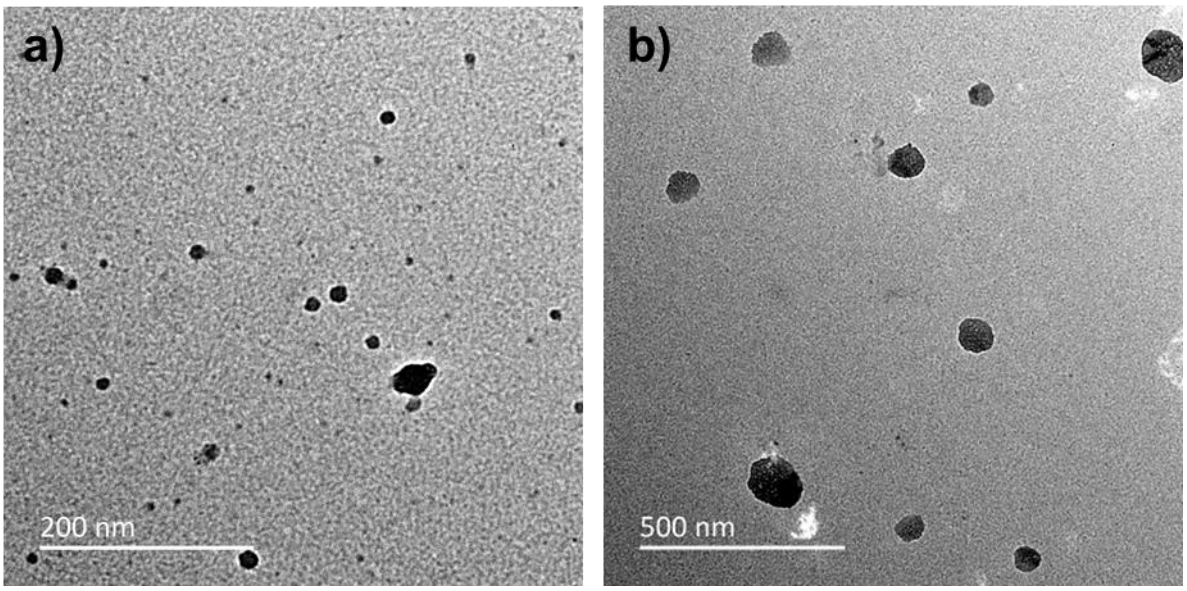

Figure S18. Dried TEM pictures of a) M1 sample (C_{pol}=10 g/L, Φ_{org}=25%) and b) particles prepared without any stabilizer.

DLS.

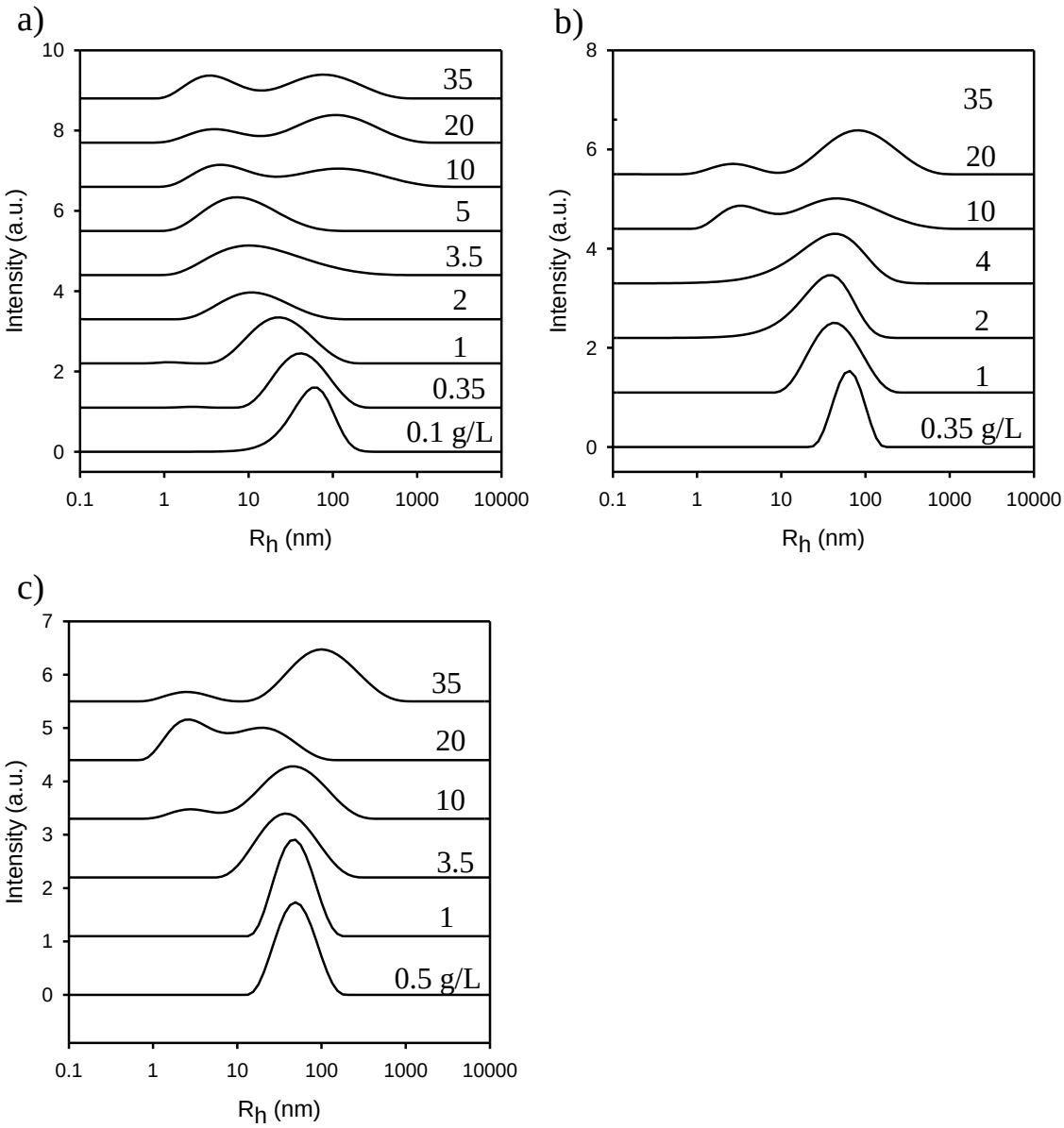

Figure S19. Distribution of sizes for a) M1, b) M2 and c) M3 samples at various polymer concentrations indicated on the figures.